Title

A visual circuit related to the nucleus reuniens for the spatial memory-promoting effects of light treatment

Authors/Affiliations

Xiaodan Huang[1,2,14], Pengcheng Huang[3,14], Lu Huang[1,2,14], Zhengfang Hu[1], Xianwei Liu[1], Jiawei Shen[4], Yue Xi[1], Yan Yang[1], Yunwei Fu[1], Qian Tao[5], Song Lin[6], Anding Xu[2], Fuqiang Xu[7], Tian Xue[4,8], Kwok-Fai So[1,9,10,11,12*], Haohong Li[3,13*], and Chaoran Ren[1,9,11,12,15*]

[1]Guangdong-Hongkong-Macau Institute of CNS Regeneration, Ministry of Education CNS Regeneration Collaborative Joint Laboratory, Jinan University, Guangzhou 510632, China
[2]Department of Neurology and Stroke Center, The First Affiliated Hospital of Jinan University, Guangzhou 510632, China
[3]Britton Chance Center for Biomedical Photonics, Wuhan National Laboratory for Optoelectronics, MoE Key Laboratory for Biomedical Photonics, Collaborative Innovation Center for Biomedical Engineering, School of Engineering Sciences, Huazhong University of Science and Technology, Wuhan 430074, China
[4]Hefei National Laboratory for Physical Sciences at the Microscale, Neurodegenerative Disorder Research Center, Chinese Academy of Sciences Key Laboratory of Brain Function and Disease, School of Life Sciences, Division of Life Sciences and Medicine, University of Science and Technology of China, Hefei 230026, China
[5]Psychology Department, School of Medicine, Jinan University, Guangzhou 510632, China
[6]Physiology Department, School of Medicine, Jinan University, Guangzhou 510632, China
[7]CAS Key Laboratory of Brain Connectome and Manipulation, the Brain Cognition and Brain Disease Institute (BCBDI), Shenzhen Institutes of Advanced Technology, Chinese Academy of Sciences (CAS), Shenzhen 518055, China
[8]Center for Excellence in Brain Science and Intelligence Technology, Chinese Academy of Sciences, Shanghai 200031, China
[9]Bioland Laboratory (Guangzhou Regenerative Medicine and Health Guangdong Laboratory), Guangzhou 510530, China
[10]Department of Ophthalmology and State Key Laboratory of Brain and Cognitive Sciences, The University of Hong Kong, Hong Kong, China
[11]Center for Brain Science and Brain-Inspired Intelligence, Guangdong-Hong Kong-Macao Greater Bay Area, Guangzhou 510515, China
[12]Co-innovation Center of Neuroregeneration, Nantong University, Nantong 226001, China
[13]The MOE Frontier Science Center for Brain Research and Brain-Machine Integration, Zhejiang University School of Brain Science and Brain Medicine, Hangzhou 310012, China
[14]These authors contributed equally
[15]Lead contact
[*]Correspondence:
hrmaskf@hku.hk (K.F.S.), hxli@hust.edu.cn (H.H.L.), tchaoran@jnu.edu.cn (C.R.R.)

SUMMARY

Light exerts profound effects on cognitive functions across species, including humans. However, the neuronal mechanisms underlying the effects of light on cognitive functions are poorly understood. In this study, we show that long-term exposure to bright light treatment promotes spatial memory through a di-synaptic visual circuit related to the nucleus reuniens (Re). Specifically, a subset of SMI-32-expressing ON-type retinal ganglion cells (RGCs) innervate CaMKIIα neurons in the thalamic ventral lateral geniculate nucleus and intergeniculate leaflet (vLGN/IGL), which in turn activate CaMKIIα neurons in the Re. Specific activation of vLGN/IGL-projecting RGCs, activation of Re-projecting vLGN/IGL neurons, or activation of postsynaptic Re neurons is sufficient to promote spatial memory. Furthermore, we demonstrate that the spatial memory-promoting effects of light treatment are dependent on the activation of vLGN/IGL-projecting RGCs, Re-projecting vLGN/IGL neurons, and Re neurons. Our results reveal a dedicated subcortical visual circuit that mediates the spatial memory-promoting effects of light treatment.

INTRODUCTION

Changes in lighting conditions exert broad effects on physiological and behavioral functions, including circadian rhythm, mood, and cognition (Fu et al., 2005; Vandewalle et al., 2009; LeGates et al., 2014). In humans, brighter illumination during the day improves cognitive performance (Baron *et al*., 1992; Heschong, 2002; Mills *et al*., 2007; Viola *et al*., 2008; Barkmann *et al*., 2012), and bright light therapy appears to attenuate cognitive deterioration in early-stage dementia (Yamadera *et al*, 2000; Riemersma-van der Lek et al., 2008; Forbes *et al*., 2009). In rodents, bright light has been shown to enhance fear and spatial memory (Warthen et al., 2011; Soler et al., 2018), whereas animals kept in dim and irregular lightening conditions showed impaired spatial memory (Soler et al., 2018; Fernandez et al., 2018). However, the neuronal circuits that underlie the effects of light on memory are still not well understood.

The nucleus reuniens (Re) of the midline thalamus is highly conserved across species, and is interconnected with the limbic systems, including the hippocampus (HPC) (Wouterlood et al., 1990; Vertes et al. 2006; Hoover and Vertes 2012; Cassel et al., 2013; Varela et al., 2014). Accumulating evidence suggest that the Re contributes to the regulation of neuronal activity in the HPC and plays a prominent role in memory processing (Loureiro et al., 2012; Cassel and Pereira de Vasconcelos, 2015; Cholvin et al., 2018; Jung et al., 2019; Hauer et al., 2019; Klein et al., 2019). Notably, the Re is a target of multiple cortical and subcortical brain regions that appears to receive sensory input via different modalities (McKenna and Vertes, 2004; Oh et al., 2014; Scheel et al., 2020), and neuronal activity in the Re can be regulated by bright light (Brown et al., 2011). The Re might therefore be important in mediating the effects of light on memory performance which depends on the HPC.

In this study, by combining conventional neurotracer and transneuronal virus tracing techniques, we identified a di-synaptic visual circuit connecting the retina and the Re in mice. In the retina, a subset of SMI-32-expressing ON-type retinal ganglion cells (RGCs) innervate CaMKIIα neurons in the ventral lateral geniculate nucleus and intergeniculate leaflet (vLGN/IGL), which in turn activate CaMKIIα neurons in the Re. The role of the retina-vLGN/IGL-Re pathway in the regulation of memory performance was investigated using an array of brain circuit interrogation tools, including c-Fos brain mapping, *in vivo* electrophysiological recording and chemogenetics. We demonstrate that activation of the retina-vLGN/IGL-Re pathway underlies the spatial memory-promoting effects of light treatment.

Light treatment promotes spatial memory performance

To evaluate the effect of light treatment on memory performance, we first kept the home cages of the control and experimental animals on different layers of a custom-designed light cabinet for 3 weeks. Cool LED lights (UV-free) with adjustable brightness were installed at the top of each floor of the cabinet, so the brightness of each floor of the cabinet could be adjusted separately. The animals in the control group (Co) were housed under a 7 AM to 7 PM 12 h:12 h light/dark cycle (~200 lux white ambient illumination). The animals in the experimental group (LT) were also housed under a 7 AM to 7 PM 12 h:12 h light/dark cycle (~200 lux white ambient illumination) except for during light treatment (~0 lux, 1000 lux, 3000 lux, or 5000 lux white ambient illumination from 8 AM to 10 AM). Then, we assessed the novel object preference and object location memory of the mice using the novel object recognition (NOR) test and novel object location (NOL) test, respectively (Figures 1A and 1B). We found that although light treatment did not significantly alter recognition index values in the NOR test (Figure 1C; Figure S1A), it promoted spatial memory assessed by the NOL test in an intensity-dependent manner (Figure S1A), as light treatment at a strength of at least 3000 lux was required to significantly promote spatial memory (Figure 1C; Figure S1A). In addition, the spatial memory-promoting effects of light treatment (3000 lux, 2 h/day, 3 weeks) could last over 2 weeks after light treatment was terminated (Figure S1B). To further confirm whether light treatment (3000 lux, 2 h/day, 3 weeks) could promote spatial memory, we next conducted the Morris water maze (MWM) to test spatial memory of the location of a hidden platform on the basis of surrounding contextual cues (Figure 1A). We subjected mice in both the Co and LT groups to a 2-day training session (3 trials/day), in which both groups identified the hidden platform over 6 successive training trials and exhibited no significant difference in escape latency (Figure 1D). During the probe trial, the mice in the LT group spent significantly more time exploring the quadrant that previously contained the platform (the target quadrant) (36.64% ± 2.94%), whereas the mice in the Co group explored the target quadrant by chance (20.39% ± 3.62%) (Figure 1E). We also found that light treatment did not significantly change the average velocity during the probe trial (Figure 1E), the optomotor response (OMR) tested under photopic and scotopic conditions (Figure 1F), or the general circadian rhythmicity assessed by the wheel-running test (WRT) (Figure 1G; Figure S1F). These results confirm that long-term exposure to bright light treatment promotes spatial memory without affecting the motor and visual functions or the circadian rhythm of mice.

Next, we further probed which aspects of light treatment are important for its spatial memory-promoting effects. To determine whether multiple days of light treatment are required to promote spatial memory, we compared the effects of 1 day, 1 week, 2 weeks, 3 weeks and 4 weeks of light treatment (3000 lux, 2 h/day) on spatial memory assessed by the NOL test and found that the spatial memory-promoting effects of light treatment appear to be dose dependent; at least 3 weeks of light treatment was needed to significantly promote spatial memory (Figure S1C). Given that the behavioral tests mentioned above were conducted in the afternoon (1 PM to 4 PM), to determine whether light treatment (3000 lux, 2 h/day, 3 weeks) could also promote spatial memory tested in a different circadian phase, we performed the NOL test at night (8 PM to 11 PM) and found that animals in the LT group also displayed better NOL performance than did the Co group at night (Figure S1D). Finally, we tested whether light treatment applied at a different time of day could also promote spatial memory by performing light treatment (3000 lux) between 1 PM and 3 PM each day for 3 weeks. We found that light treatment administered during the afternoon also significantly promoted spatial memory (Figure S1E).

The Re is required for the spatial memory-promoting effects of light treatment

Given that spatial memory evaluated in the NOL and MWM tests is highly HPC-dependent and that synchronous neuronal activity in the HPC is relevant to spatial memory operations (Redish and Touretzky, 1998; Broadbent et al., 2006; Barker and Warburton, 2011), we next probed whether light treatment could promote spatial memory accompanied by changed synchronous neuronal activity in the HPC. We first exposed the animals to 3 weeks of light treatment (3000 lux, 8 AM to 10 AM), then recorded the local field potentials (LFPs) from the CA1 of the dorsal HPC as the animals performed the NOL test (Figure 2A). We found that gamma oscillation in the CA1 during exploration of the novel location was significantly increased in the LT group (Figures 2B-2D). In contrast, HPC oscillations in the theta and beta ranges were comparable between the Co and LT groups (Figures 2B-2D). In addition, we found that c-Fos expression in the HPC was significantly increased after 3 weeks of light treatment (Figure S2A), which further suggests that long-term exposure to light treatment could affect the neuronal activity in the HPC.

To determine the potential brain regions through which light treatment could promote spatial memory and increase HPC gamma oscillation, we examined the effects of long-term exposure to light treatment (3000 lux, 8 AM to 10 AM, 3 weeks) on c-Fos expression throughout the brain. In addition to the increased c-Fos expression in visual related-brain regions including the vLGN/IGL and superior colliculus (SC) (Figure S2A), c-Fos expression in the ventral midline thalamic Re was also significantly increased after 3 weeks of light treatment (Figure 2E). Given that growing evidence indicates that the Re is implicated in the regulation of HPC function and spatial memory operation (Loureiro et al., 2012; Cassel and Pereira de Vasconcelos, 2015; Cholvin et al., 2018; Jung et al., 2019; Hauer et al., 2019; Klein et al., 2019), we postulated that long-term exposure to light treatment might promote spatial memory and increase HPC gamma oscillation by modulating neuronal activity in the Re. To test this possibility, we first examined the effects of long-term exposure to light treatment (3000 lux, 8 AM to 10 AM, 3 weeks) on the intrinsic physiological properties of Re neurons. We found that the current-evoked action potentials, spontaneous firing rate, frequency and amplitude of the miniature excitatory postsynaptic currents (mEPSCs) of Re neurons were significantly increased in mice that received long-term exposure to light treatment (Figures 2F-2H), suggesting that long-term exposure to light treatment can increase the excitability of Re neurons by enhancing the excitatory inputs to the Re. Next, we evaluated whether the Re is required for light treatment to promote spatial memory and HPC gamma oscillation by globally silencing Re neurons with tetanus neurotoxin (TetTox), a molecular tool for synaptic inactivation (Xu and Südhof, 2013). Three weeks of light treatment (3000 lux, 8 AM to 10 AM) was conducted 2 weeks after the injection of AAV2/9-hSyn-TetTox-eYFP in the Re (Figures 2I and 2J). We found that global inactivation of the Re abolished the effects of light treatment on spatial memory and HPC gamma oscillation (Figures 2K-2M). In addition, we found that without light treatment inactivation of the Re did not significantly alter the spatial memory assessed by the NOL test (Figure S2C). These results indicate that activation of the Re is required for light treatment to promote spatial memory and increase HPC gamma oscillation.

Activation of Re-projecting vLGN/IGL neurons is required for the spatial memory-promoting effects of light treatment

In mammals, the retina is the only sensory organ directly responsive to light, and there is no evidence that RGCs can directly innervate the Re (Martersteck et al., 2017). Thus, the regulatory effects of light treatment on neuronal activity in the Re should be mediated by other brain regions located in the visual pathway. To determine the potential brain regions that might transmit light signals to the Re, we used a transsynaptic tracing method based on a modified rabies virus to examine the vision-related brain regions that could directly innervate the Re. Re neurons were first infected with AAV expressing the rabies glycoprotein and histone-tagged EGFP (Helper), which is required for the replication of rabies virus (Figures 3A and 3B). Next, SAD-ΔG-DsRed (EnvA) (RV-DsRed) was injected into the Re to infect Helper$^+$ Re neurons (Figures 3A-3C). The double-infected rabies-DsRed$^+$/Glyco-EGFP$^+$ Re neurons (starter cells) produced infectious ΔG-rabies-DsRed that propagated transneuronally to infect the neurons that formed synapses with them (Figures 3B and 3C). In addition to the well-characterized Re input from the medial prefrontal cortex (mPFC) (Vertes et al. 2006; Cassel et al., 2013; Varela et al., 2014; Figure 3C), we found that vision-related brain regions, including the vLGN/IGL and SC, showed convergence onto Re neurons (Figure 3C). Furthermore, c-Fos expression in both the vLGN/IGL and SC was significantly increased after long-term exposure to light treatment (Figure S2A). These results suggest that light treatment might regulate neuronal activity in the Re through activating the vLGN/IGL and SC.

To explore which vision-related brain region might be important for the spatial memory-promoting effects of light treatment, we measured the spatial memory in the NOL and MWM tests after chemogenetic inhibition of Re-projecting vLGN/IGL neurons and Re-projecting SC neurons, respectively, during light treatment (Figure 3D). We first delivered the monosynaptic retrograde transport virus rAAV2/2-Retro-Cre (Tervo et al., 2016) into the Re (Figure S3A) and infected Re-projecting vLGN/IGL neurons with a Cre-dependent virus encoding the neuronal inhibitor DREADD hM4Di (AAV2/9-DIO-hM4Di-mCherry) (Figure 3E). Three weeks of light treatment (3000 lux, 8 AM to 10AM) was conducted 2 weeks after the virus injection, in which light treatment was performed every day 30 min after i.p. injection of clozapine N-oxide (CNO, 1 mg/kg) (Figure 3D; Figure S3B). We found that chemogenetic inhibition of Re-projecting vLGN/IGL neurons significantly impaired the spatial memory-promoting effects of light treatment (Figure 3F; Figure S3C). In contrast, chemogenetic inhibition of Re-projecting SC neurons did not significantly alter the spatial memory-promoting effects of light treatment (Figures 3G and 3H; Figures S3B and S3D). In addition, we found that without light treatment inactivation of Re-projecting vLGN/IGL neurons or Re-projecting SC neurons did not significantly alter the spatial memory assessed by the NOL and MWM tests (Figure S3E and S3F). The above results indicate that activation of the vLGN/IGL but not the SC is required for the spatial memory-promoting effects of light treatment.

vLGN/IGL neurons activate Re neurons through direct projections

To determine how the vLGN/IGL regulates neuronal activity in the Re, we delivered rAAV2/2-Retro-Cre into the Re of C57BL/6 mice and a Cre-dependent virus encoding channelrhodopsin-2 and mCherry (AAV2/9-DIO-ChR2-mCherry) into the vLGN/IGL (Figure 4A; Figure S4A). Next, we optogenetically activated vLGN/IGL-Re projections and recorded postsynaptic currents from Re neurons (Figure 4B). Optogenetically activating vLGN/IGL-Re projections evoked exclusively excitatory postsynaptic currents (EPSCs) in 39.68% of recorded neurons, but both EPSCs and inhibitory postsynaptic currents (IPSCs) in 36.51% of recorded neurons, in which the amplitude of EPSCs was higher than that of IPSCs (Figures 4C). Besides, the recorded postsynaptic currents were completely blocked by the application of TTX and recovered by the application of TTX/4-AP (Figure 4D), indicating that the postsynaptic currents recorded in Re neurons were elicited by direct synaptic connections between Re-projecting vLGN/IGL neurons and the recorded Re neurons. Furthermore, the excitatory effects of vLGN/IGL-Re projections could be blocked by the AMPA/kainate receptor antagonist NBQX, while the inhibitory effects could be blocked by the $GABA_A$ receptor antagonist picrotoxin (PTX) (Figure 4E). In addition, we found that all recorded Re neurons that could respond to blue light stimulation were CaMKIIα neurons, which could further project to the CA1 of the HPC and medial entorhinal cortex (MEC) (Figure 4B; Figures S4B and S4C). These results indicate that vLGN/IGL neurons transmit predominantly excitatory input to Re CaMKIIα neurons. To determine whether vLGN/IGL excitatory neurons could directly innervate the Re, we delivered a virus encoding a red fluorescent protein, mCherry (AAV2/9-CaMKIIα-mCherry), into the vLGN/IGL of C57BL/6 mice to selectively infect CaMKIIα neurons, after which we injected green fluorescent latex microspheres (retrobeads) into the Re to label Re-projecting vLGN/IGL neurons in a retrograde manner (Figure S4D). We found that approximately 94.1% of retrobeads-labeled Re-projecting neurons were colabeled with mCherry (Figure S4E). The above results indicate that a subset of vLGN/IGL CaMKIIα neurons activate Re CaMKIIα neurons through direct projections.

Long-term activation of the vLGN/IGL-Re pathway promotes spatial memory

In light of our finding that activation both Re neurons and Re-projecting vLGN/IGL neurons is required for the spatial memory-promoting effects of long-term exposure to light treatment, we tested whether long-term activation of the vLGN/IGL-Re pathway could also promote spatial memory. We first delivered rAAV2/2-Retro-Cre into the Re and bilaterally infected Re-projecting vLGN/IGL neurons with a Cre-dependent virus encoding the neuronal activator DREADD hM3Dq (AAV2/9-DIO-hM3Dq-mCherry) (Figure 5A). The Re-projecting vLGN/IGL neurons were activated daily via i.p. injection of CNO (1 mg/kg) for 3 weeks (Figures 5B and 5C). Long-term activation of Re-projecting vLGN/IGL neurons significantly promoted spatial memory in the NOL and MWM tests (Figures 5D and 5E; Figures S5A and S5B), which was accompanied by increased excitability of Re neurons (Figures 5F and 5G; Figure S5C). In addition, long-term activation of Re-projecting vLGN/IGL neurons also significantly increased HPC gamma oscillation during the NOL test (Figures 5H and 5I).

To further confirm whether long-term activation of the vLGN/IGL-Re pathway is sufficient to promote spatial memory, we next injected the monosynaptic anterograde transport virus AAV2/1-Cre (Zingg et al., 2017) into the bilateral vLGN/IGL (Figure S6A) and infected Re postsynaptic neurons with AAV2/9-DIO-hM3Dq-mCherry (Figure 6A). The Re neurons that received direct innervations from the vLGN/IGL were activated daily for 3 weeks (Figures 6B and 6C). We found that long-term activation of Re neurons receiving direct vLGN/IGL input also significantly promoted spatial memory and increased the excitability of Re neurons and HPC gamma oscillation (Figures 6D-6H; Figures S6B-S6D). Thus, long-term activation of the vLGN/IGL-Re pathway is sufficient to promote spatial memory.

Activation of vLGN/IGL-projecting RGCs is required for the spatial memory-promoting effects of light treatment

It is well established that the vLGN/IGL receives direct retinal inputs (Harrington, 1997; Huang et al., 2019). To determine whether RGCs could directly innervate the vLGN/IGL-Re pathway, we delivered rAAV2/2-Retro-Cre into the Re and infected Re-projecting vLGN/IGL neurons with AAV expressing the rabies glycoprotein and Helper (Figures 7A and 7B). Twenty-one days later, we injected SAD-ΔG-DsRed (EnvA) (RV-DsRed) into the vLGN/IGL to infect Helper$^+$ Re-projecting vLGN/IGL neurons (Figures 7A and 7B). The double-infected rabies-DsRed$^+$/Glyco-EGFP$^+$ vLGN/IGL relay neurons (starter cells) produced infectious ΔG-rabies-DsRed that propagated transneuronally to infect the RGCs that formed synapses with them (Figures 7B-7D). In the retina, 873 ± 42 RGCs were labeled with rabies virus (n = 4 retinas, Figures 7D). We found that approximately 91.2% of rabies virus-labeled RGCs were immunopositive for SMI-32 and exhibited morphological features similar to ON-type RGCs (Figures 7D). Next, we assessed the receptive field (RF) centers and the dynamics of the light response of 15 rabies virus-labeled RGCs. To assess the RF centers of the recorded RGCs, a circular light spot (3.2 x 10^{10} photons/cm^2/s) centered on the cell body was flashed on and off periodically (1 s on/1 s off). The spot size gradually increased (spot diameters: 10, 40, 70, 140, 200, 250 and 310 μm). The spot size that could evoke the maximum discharge was accepted as covering the RF center (Figure 7E). We found that the size of the RF center was similar for all the recorded RGCs: ~200-250 μm in diameter (Figure 7E). To assess the dynamics of the light response of the recorded RGCs, we inspected the time course of the firing rate under a 1 s light spot (3.2 x 10^{10} photons/cm^2/s) with a size equal to the RF center of the recorded RGC. We found that all the recorded RGCs responded with sustained depolarization to a 1 s light spot, and the latency from light onset to peak firing rate and the peak firing rate were similar across the recorded RGCs (Figure 7F). The above results suggest that a subset of SMI-32$^+$ ON-type RGCs with similar light response properties directly innervate the vLGN/IGL-Re pathway.

Given that the excitatory neurotransmitter glutamate is considered to be the neurotransmitter of most RGCs (Finlayson and Iezzi, 2010), and in view of our finding that long-term activation of the vLGN/IGL-Re pathway promotes spatial memory (Figures 5 and 6), we tested the effects of long-term activation of the vLGN/IGL-projecting RGCs on spatial memory. We found that 3 weeks of chemogenetic activation of vLGN/IGL-projecting RGCs significantly promoted spatial memory in the NOL and MWM tests (Figures 7G-7K; Figures S7A and S7B), accompanied by increased HPC gamma oscillation (Figures S7C and S7D). In addition, long-term activation of vLGN/IGL-projecting RGCs also significantly increased the excitability of Re neurons and enhanced excitatory inputs to Re neurons (Figures S7E-S7G). These results indicate that long-term activation of vLGN/IGL-projecting RGCs promotes spatial memory.

Finally, we evaluated the contribution of vLGN/IGL-projecting RGCs to the spatial memory-promoting effects of light treatment. We delivered rAAV2/2-Retro-Cre into the bilateral vLGN/IGL, and infected vLGN/IGL-projecting RGCs with AAV2/9-DIO-hM4Di-mCherry through intraocular injection (Figures 8A and 8B). Three weeks of light treatment (3000 lux, 8 AM to 10 AM) was conducted 2 weeks after the virus injection, during which light treatment was performed every day 30 min after i.p. injection of CNO (1 mg/kg) (Figures 8B and 8C). Inhibition of vLGN/IGL-projecting RGCs eliminated the spatial memory-promoting effects of light treatment (Figures 8D and 8E; Figures S8). Thus, activation of vLGN/IGL-projecting RGCs is required for the spatial memory-promoting effects of light treatment.

DISCUSSION

Light signals transmitted by the retina are a powerful modulator of non-image-forming functions, including superior cognitive performance (Fu et al., 2005; Vandewalle et al., 2009; LeGates et al., 2014). Accumulating evidence has found that brighter illumination can not only alleviate depressive-like behaviors but also improve cognitive performance across species, including humans (Baron et al., 1992; Heschong, 2002; Mills et al., 2007; Viola et al., 2008; Barkmann et al., 2012; Yamadera et al, 2000; Riemersma-van der Lek et al., 2008; Forbes et al., 2009; Warthen et al., 2011; Soler et al., 2018). However, the precise neuronal circuits that underlie the beneficial effects of light on cognitive functions remain to be elucidated. In this study, we provide direct evidence that long-term exposure to bright light treatment, a non-drug treatment mainly used in the treatment of depression, can also improve spatial memory through a di-synaptic visual circuit linking the retina and the Re.

HPC gamma oscillation is associated with numerous higher-order cognitive functions, including spatial memory operations (Fries, 2009; Colgin and Moser, 2010; Colgin, 2016). Consistent with this view, we found that long-term exposure to light treatment improved spatial memory accompanied by increased HPC gamma oscillation. It is well documented that the HPC is not a retinorecipient brain region (Martersteck et al., 2017). The modulatory effects of light treatment on spatial memory and HPC gamma oscillation should be achieved through brain regions that could be directly regulated by light treatment. Our data support this proposal, revealing that the Re of the ventral midline thalamus could be directly activated by light treatment and that silencing Re neurons abolished the effects of light treatment on both spatial memory and HPC gamma oscillation. The exact mechanisms underlying the effects of light treatment on HPC gamma oscillation are still unknown. Given that the MEC plays an important role in the generation of CA1 fast gamma oscillation (Colgin et al., 2009; Yamamoto et al., 2014), and in light of our finding that Re neurons receiving direct vLGN/IGL inputs could further project to the MEC (Figures S4B and S4C), light treatment might regulate CA1 fast gamma oscillation through the vLGN/IGL-Re-MEC-CA1 pathway. On the other hand, we also found that Re neurons receiving direct vLGN/IGL input could also directly innervate the CA1 of the HPC (Figures S4B and S4C). Given that much evidence indicates that inhibitory interneurons in the CA1 are crucial for the generation of gamma oscillation (Bartos et al., 2007; Colgin, 2016), and combined with previous findings that Re-HPC projections could regulate neuronal activity in CA1 interneurons (Dolleman-Van der Weel et al., 1997, 2000), it is also possible that the vLGN/IGL-Re-HPC pathway is involved in the regulation of HPC gamma oscillation by light treatment.

Although the Re does not receive direct retinal inputs (Martersteck et al., 2017), neuronal activity in the Re can be activated by bright light (Brown et al., 2011). Consistently, we found that long-term exposure to light treatment not only activated the Re, but also enhanced the excitatory inputs to Re neurons and consequentially promoted their excitability. The above results suggest that light treatment signals could be transmitted to the Re through certain visual pathways. Accordingly, we demonstrated that the vLGN/IGL could directly innervate the Re and that activation of the vLGN/IGL is needed for the spatial memory-promoting effects of light treatment. Although projection of the visual thalamus to the Re has been proposed across species (Kawamura et al., 1978; Morin and Blanchard, 1999; McKenna and Vertes, 2004; Scheel et al., 2020), the morphological and physiological properties of this pathway are still unclear. It is well established that the vLGN/IGL is enriched with GABA neurons (Harrington, 1997; Sabbagh et al., 2020), and our previous study found that a subset of vLGN/IGL GABA neurons could send dense projections to the lateral habenula (LHb) (Huang et al., 2019). In addition, results derived from genome-wide atlas of the mouse brain suggest that the vLGN/IGL also contain CaMKIIα neurons (Lein et al., 2007). Consistently, we found that the Re-projecting vLGN/IGL neurons were CaMKIIα$^+$ (Figures S4D and S4E), which could send dense projections to several subcortical brain regions, including the Re, anterior pretectal nucleus (APN) and lateral posterior nucleus of the thalamus (LP), send moderate projections to the SC, but send weak projections to the suprachiasmatic nucleus (SCN), LHb and olivary pretectal nucleus (OPN) (Figure S4A). These results suggest that there is cellular heterogeneity within the vLGN/IGL and that Re-projecting vLGN/IGL neurons represent a subset of vLGN/IGL neurons with unique projection patterns. Furthermore, we demonstrated the vLGN/IGL could activate the Re through direct projections. Combined these results with our finding that long-term exposure to light treatment increased the excitability of Re neurons accompanied by improved spatial memory and increased HPC gamma oscillation, it is highly likely that long-term activation of the vLGN/IGL-Re pathway is also sufficient to promote spatial memory and increase HPC gamma oscillation. Our data support this proposal revealing that both long-term activation of Re-projecting vLGN/IGL neurons and activation of Re neurons receiving direct vLGN/IGL innervations significantly promoted spatial memory and increased HPC gamma oscillation.

Using the modified rabies virus retrograde tracing technique, we found that a subset of SMI-32$^+$ ON-type RGCs directly innervate the vLGN/IGL-Re pathway. As axon terminals of RGCs release the excitatory neurotransmitter glutamate (Finlayson and Iezzi, 2010), it is reasonable to postulate that information regarding light treatment transmitted by those RGCs could promote spatial memory. In support of this view, we demonstrated that specific inhibition of vLGN/IGL-projecting RGCs during light treatment abolished the spatial memory-promoting effects of light treatment. Furthermore, long-term activation of vLGN/IGL-projecting RGCs also promoted spatial memory and HPC gamma oscillation, suggesting that long-term activation of vLGN/IGL-projecting RGCs is also sufficient for the improvement of spatial memory. Interestingly, the morphological and physiological features of the RGCs innervating the vLGN/IGL-Re pathway strongly resemble those of the RGCs that innervate the vLGN/IGL-LHb pathway, which also express SMI-32 and spike at light onset (Huang et al., 2019). Given that RGCs innervating the vLGN/IGL-LHb pathway underlies the anti-depressive effects of light treatment (Huang et al., 2019), it seems that SMI-32$^+$ ON-type RGCs could underlie both the anti-depressive and spatial memory-promoting effects of light treatment.

A recent study found that gamma entrainment using sensory stimulus (GENUS) reduced the amyloid load in the HPC and improved spatial memory in 6-month-old 5xFAD mice (Martorell et al., 2019). Here, we found that long-term exposure to light treatment promoted spatial memory and increased HPC gamma oscillation during the NOL test in C57BL/6 mice. One might expect that long-term exposure to light treatment should also improve spatial memory in 6-month-old 5xFAD mice. However, we found that long-term exposure to light treatment did not significantly promote spatial memory in 6-month-old 5xFAD mice (Figures S9A-S9C). In addition, unlike GENUS, bright light (3000 lux) alone could not directly increase gamma oscillation in the HPC (Figures S9D-S9F). The HPC gamma oscillation detected during the NOL test maybe too weak to reduce the amyloid load and reverse the deficits in spatial memory of 5xFAD mice. On the other hand, GENUS did not show beneficial effects on spatial memory performance in WT mice (Martorell et al., 2019), which further suggests that the neuronal mechanisms underlying the spatial memory-promoting effects of light treatment and GENUS are different.

Using depressive-like mouse models, our previous study found that exposure to 2 weeks of light treatment (3000 lux, 2 h/day) significantly reduced depressive-like behaviors but tended to increase anxiety-like behaviors (Huang et al., 2019). In this study, we also conducted the open field test (OFT) and sucrose preference test (SPT) to measure the effects of exposure to 3 weeks of light treatment (3000 lux, 2 h/day) on anxiety- and depressive-like behaviors, respectively. We found that exposure to 3 weeks of light treatment significantly increased anxiety-like behaviors assessed by the OFT but did not significantly affect the depressive-like behaviors assessed by the SPT (Figures S9G). Given that increased arousal is among the earliest events observed in a state of anxiety (Gray and McNaughton, 1996; Milosavljevic et al., 2016), our results suggest that light treatment can affect arousal. Based on this finding, it is reasonable for one to speculate that light treatment might primarily change arousal with alterations in spatial memory as one consequence. However, our data do not support this proposal. First, we found that inhibition of Re neurons or Re-projecting vLGN/IGL neurons significantly impaired the spatial memory-promoting effects of light treatment (Figures 2J and 2K, 3E and 3F) but not the arousal and/or anxiety-evoking effects of light treatment (Figures S9H and S9I). Second, we tested the response of mice to bright light (1000 lux) when challenged with the OFT and NOL test. We found that in bright light, the mice exhibited significantly increased arousal and/or anxiety-like behaviors assessed by the OFT (Figure S9J), whereas the spatial memory assessed by the NOL test was not significantly altered (Figure S9K). The above results suggest that the circuit mechanisms underlying the spatial memory-promoting effects and arousal/anxiety-evoking effects of light treatment are not exactly the same and that the effects of light treatment on behavioral state are not necessarily the direct cause of the spatial memory-promoting effects of light treatment.

In summary, our study shows that the retina, vLGN/IGL, and Re are crucial elements of the neuronal circuitry for the spatial memory-promoting effects of light treatment. Given the high conservation of SMI-32$^+$ ON-type RGCs, the visual thalamus and the Re in rodents and humans, these novel results may improve our current understanding of the mechanisms underlying the effects of light on memory.

ACKNOWLEDGMENTS

We thank Dr. Minmin Luo (National Institute of Biological Sciences, China) and Dr. Wenbiao Gan (New York University) for critical comments on the manuscript, Dr. Lingqiang Zhu (Huazhong University of Science and Technology, China) for providing the 5xFAD mice. We also thank Drs. Gong Chen, Wenliang Lei, Sen Yan and Yibo Qu at Jinan University for their technical support. C.R. is supported by National Natural Science Foundation of China (31922030, 31771170), Science and Technology Program of Guangdong (2018B030334001), Guangdong Special Support Program (2017TQ04R173), Science and Technology Program of Guangzhou, China (202007030012), Pearl River S&T Nova Program of Guangzhou (201806010198), Shenzhen Basic Research Grant (JCYJ20170412164259361). H.L. is supported by National Natural Science Foundation of China (31671105). L.H. is supported by National Natural Science Foundation of China (31900720), Guangdong Natural Science Foundation (2019A1515011598). K.S. is supported by Programme of Introducing Talents of Discipline to Universities (B14036).

AUTHOR CONTRIBUTIONS

C.R. conceived the idea and wrote the manuscript. C.R., H.L. and K.S. designed experiments. X.H., C.H. and J.S. performed behavioral experiments and in vivo activity recordings. L.H. and Y.Y.

performed surgery. X.H. and Z.H. performed physiological recordings. X.H., Y.X. X.L. and Y.F. performed histology and microscopy. C.R., X.H., C.H., Q.T. T.X., A.X. F.X. and S.L. analyzed the data.

DECLARATION OF INTERESTS

The authors declare no competing interests.

REFERENCES

1. Barker, G.R., and Warburton, E.C. (2011). When is the hippocampus involved in recognition memory? J Neurosci *31*, 10721-31.

2. Barkmann, C., Wessolowski, N., Schulte-Markwort, M. (2012). Applicability and efficacy of variable light in schools. Physiol. Behav *105*, 621–627.

3. Baron, R., Rea, M., Daniels, S. (1992). Effects of indoor lighting (illuminance and spectral distribution) on the performance of cognitive tasks and interpersonal behaviors: the potential mediating role of positive affect. Motiv. Emot *16*, 1–33.

4. Bartos, M., Vida, I., Jonas, P. (2007). Synaptic mechanisms of synchronized gamma oscillations in inhibitory interneuron networks. Nat Rev Neurosci *8*, 45-56.

5. Broadbent, N.J., Squire, L.R., Clark, R.E. (2006). Reversible hippocampal lesions disrupt water maze performance during both recent and remote memory tests. Learn Mem *13*, 187-91.

6. Brown, T.M., Wynne, J., Piggins, H.D., Lucas, R.J. (2011). Multiple hypothalamic cell populations encoding distinct visual information. J Physiol *589*, 1173-94.

7. Cassel, J.C., Pereira, de. Vasconcelos. A., Loureiro, M., Cholvin, T., Dalrymple-Alford, J.C., Vertes, R.P. (2013). The reuniens and rhomboid nuclei: neuroanatomy, electrophysiological characteristics and behavioral implications. Progress in neurobiology *111*, 34-52.

8. Cassel, J.C., Pereira, de. Vasconcelos. A. (2015). Importance of the ventral midline thalamus in driving hippocampal functions. Prog Brain Res *219*, 145-61.

9. Chen, X., and Li, H. (2017). ArControl: An Arduino-Based Comprehensive Behavioral Platform with Real-Time Performance. Front Behav Neurosci *11*, 244.

10. Cholvin, T., Hok, V., Giorgi, L., Chaillan, F.A., Poucet, B. (2018). Ventral Midline Thalamus Is Necessary for Hippocampal Place Field Stability and Cell Firing Modulation. J Neurosci *38*, 158-172.

11. Colgin, L.L. (2016). Rhythms of the hippocampal network. Nat Rev Neurosci *17*, 239-49.

12. Colgin, L.L., Denninger, T., Fyhn, M., Hafting, T., Bonnevie, T., Jensen, O., Moser, M.B., Moser, E.I. (2009). Frequency of gamma oscillations routes flow of information in the hippocampus. Nature *19*, 353-7.

13. Colgin, L.L., and Moser, E.I. (2010). Gamma oscillations in the hippocampus. Physiology (Bethesda) *25*, 319-29.

14. Dolleman-Van, der. Weel. M.J., Lopes, da. Silva. F.H., Witter, M.P. (1997). Nucleus reuniens thalami modulates activity in hippocampal field CA1 through excitatory and inhibitory mechanisms. J Neurosci *17*, 5640-50.

15. Dolleman-Van, der. Weel. M.J., Witter, M.P. (2000). Nucleus reuniens thalami innervates gamma aminobutyric acid positive cells in hippocampal field CA1 of the rat. Neurosci Lett *278*, 145-8.

16. Fernandez, D.C., Fogerson, P.M., Lazzerini, Ospri. L., Thomsen, M.B., Layne, R.M., Severin, D., Zhan, J., Singer, J.H., Kirkwood, A., Zhao, H., et al. (2018). Light Affects Mood and Learning through Distinct Retina-Brain Pathways. Cell *175*, 71-84.

17. Finlayson, P.G., and Iezzi, R. (2010). Glutamate stimulation of retinal ganglion cells in normal and s334ter-4 rat retinas: a candidate for a neurotransmitter-based retinal prosthesis. Invest Ophthalmol Vis Sci *51*, 3619-28.

18. Forbes, D., Culum, I., Lischka, A.R., Morgan, D.G., Peacock, S., Forbes, J., Forbes, S. (2009). Light therapy for managing cognitive, sleep, functional, behavioural, or psychiatric disturbances in dementia. Cochrane Database Syst. Rev *4*, CD003946.

19. Fries, P. (2009). Neuronal gamma-band synchronization as a fundamental process in cortical computation. Annu Rev Neurosci *32*, 209-24.

20. Fu, Y., Liao, H.W., Do, M.T., Yau, K.W. (2005). Non-image-forming ocular photoreception in vertebrates. Curr. Opin. Neurobiol *15*, 415–422.

21. Gray, J.A., and McNaughton, N. (1996). The neuropsychology of anxiety: reprise. Nebr. Symp. Motiv. *43*, 61–134.

22. Harrington, M.E. (1997). The ventral lateral geniculate nucleus and the intergeniculate leaflet:

interrelated structures in the visual and circadian systems. Neurosci Biobehav Rev *21*, 705-27.

23. Hauer, B.E., Pagliardini, S., Dickson, C.T. (2019). The Reuniens Nucleus of the Thalamus Has an Essential Role in Coordinating Slow-Wave Activity between Neocortex and Hippocampus. eNeuro *17*, 6.

24. Heschong, L., Wright, R., Okura, S., Klein, P., Simner, M., Berman, S., Clear, R. (2002). Daylighting impacts on human performance in school. J. Illum. Eng. Soc *31*, 101–114.

25. Hoover, W.B., and Vertes, R.P. (2012). Collateral projections from nucleus reuniens of thalamus to hippocampus and medial prefrontal cortex in the rat: a single and double retrograde fluorescent labeling study. Brain Struct Funct *217*, 191-209.

26. Huang, L., Xi, Y., Peng, Y., Yang, Y., Huang, X., Fu, Y., Tao, Q., Xiao, J., Yuan, T., An, K., et al. (2019). A Visual Circuit Related to Habenula Underlies the Antidepressive Effects of Light therapy. Neuron *102*, 128-142.

27. Jung, D., Huh, Y., Cho, J. (2019). The Ventral Midline Thalamus Mediates Hippocampal Spatial Information Processes upon Spatial Cue Changes. J Neurosci *39*, 2276-2290.

28. Kawamura, S., Fukushima, N., Hattori, S., Tashiro, T. (1978). A ventral lateral geniculate nucleus projection to the dorsal thalamus and the midbrain in the cat. Exp Brain Res *31*, 95-106.

29. Klein, M.M., Cholvin, T., Cosquer, B., Salvadori, A., Le, Mero. J., Kourouma, L., Boutillier, A.L., Pereira, de. Vasconcelos. A., Cassel, J.C. (2019). Ventral midline thalamus lesion prevents persistence of new (learning-triggered) hippocampal spines, delayed neocortical spinogenesis, and spatial memory durability. Brain Struct Funct *224*, 1659-1676.

30. LeGates, T.A., Fernandez, D.C., Hattar, S. (2014). Light as a central modulator of circadian rhythms, sleep and affect. Nat Rev Neurosci *15*, 443-54.

31. Lein, E.S., Hawrylycz, M.J., Ao, N., Ayres, M., Bensinger, A., Bernard, A., Boe, A.F., Boguski, M.S., Brockway, K.S., Byrnes, E.J., et al. (2007). Genome-wide atlas of gene expression in the adult mouse brain. Nature *445*, 168-76.

32. Loureiro, M., Cholvin, T., Lopez, J., Merienne, N., Latreche, A., Cosquer, B., Geiger, K., Kelche, C., Cassel, J.C., Pereira, de. Vasconcelos. A. (2012). The ventral midline thalamus (reuniens and rhomboid nuclei) contributes to the persistence of spatial memory in rats. J Neurosci *32*, 9947-59.

33. Martersteck, E.M., Hirokawa, K.E., Evarts, M., Bernard, A., Duan, X., Li, Y., Ng, L., Oh, S.W., Ouellette, B., Royall, J.J., et al. (2017). Diverse Central Projection Patterns of Retinal Ganglion Cells. Cell Rep *18*, 2058-2072.

34. Martorell, A.J., Paulson, A.L., Suk, H.J., Abdurrob, F., Drummond, G.T., Guan, W., Young, J.Z., Kim, D.N., Kritskiy, O., Barker, S.J., et al. (2019). Multi-sensory Gamma Stimulation Ameliorates Alzheimer's-Associated Pathology and Improves Cognition. Cell *177*, 256-271.

35. McKenna, J.T., and Vertes, R.P. (2004). Afferent projections to nucleus reuniens of the thalamus. J Comp Neurol *480*, 115-42.

36. Mills, P., Tomkins, S., Schlangen, L. (2007). The effect of high correlated colour temperature office lighting on employee wellbeing and work performance. J. Circadian Rhythms *5*, 2–10.

37. Milosavljevic, N., Cehajic-Kapetanovic, J., Procyk, C.A., Lucas, R.J. (2016). Chemogenetic Activation of Melanopsin Retinal Ganglion Cells Induces Signatures of Arousal and/or Anxiety in Mice. Curr Biol *26*, 2358-63.

38. Morin, L.P., and Blanchard, J.H. (1999). Forebrain connections of the hamster intergeniculate leaflet: comparison with those of ventral lateral geniculate nucleus and retina. Vis Neurosci *16*, 1037-54.

39. Oh, S.W., Harris, J.A., Ng, L., Winslow, B., Cain, N., Mihalas, S., Wang, Q., Lau, C., Kuan, L., Henry, A.M., et al. (2014). A mesoscale connectome of the mouse brain. Nature *508*, 207-14.

40. Redish, A.D., and Touretzky, D.S. (1998). The role of the hippocampus in solving the Morris water maze. Neural Comput *10*, 73-111.

41. Riemersma-van der Lek, R.F., Swaab, D.F., Twisk, J., Hol, E.M., Hoogendijk, W.J., Van Someren, E.J. (2008). Effect of bright light and melatonin on cognitive and noncognitive function in elderly residents of group care facilities: a randomized controlled trial. JAMA *299*, 2642–2655.

42. Sabbagh, U., Govindaiah, G., Somaiya, R.D., Ha, R.V., Wei, JC., Guido, W., Fox, M.A. (2020). Diverse GABAergic neurons organize into subtype-specific sublaminae in the ventral lateral geniculate nucleus. J Neurochem *10*.1111/jnc.15101.

43. Scheel, N., Wulff, P., de Mooij-van, Malsen, J.G. (2020). Afferent connections of the thalamic nucleus reuniens in the mouse. J Comp Neurol *528*,1189-1202.

44. Soler, J.E., Robison, A.J., Nunez, A.A., Yan, L. (2018). Light modulates hippocampal function and spatial learning in a diurnal rodent species: a study using male Nile grass rat (Arvicanthis niloticus). Hippocampus *28*, 189–200.

45. Tervo, D.G., Hwang, B.Y., Viswanathan, S., Gaj, T., Lavzin, M., Ritola, K.D., Lindo, S., Michael, S., Kuleshova, E., Ojala, D., et al. (2016). A Designer AAV Variant Permits Efficient Retrograde Access to Projection Neurons. Neuron *92*, 372-382.

46. Varela, C., Kumar, S., Yang, J.Y., Wilson, M.A. (2014). Anatomical substrates for direct interactions between hippocampus, medial prefrontal cortex, and the thalamic nucleus reuniens. Brain Struct Funct *219*, 911-29.

47. Vandewalle, G., Maquet, P., Dijk, D.J. (2009). Light as a modulator of cognitive brain function. Trends Cogn Sci *13*, 429-38.

48. Vertes, R.P., Hoover, W.B., Do, Valle. A.C., Sherman, A., Rodriguez, J.J. (2006). Efferent projections of reuniens and rhomboid nuclei of the thalamus in the rat. J Comp Neurol *499*, 768-796.

49. Viola, A.U., James, L.M., Schlangen, L.J., Dijk, D.J. (2008). Blue-enriched white light in the workplace improves self-reported alertness, performance and sleep quality. Scand. J. Work Environ. Health *34*, 297–306.

50. Warthen, D.M., Wiltgen, B.J., Provencio, I. (2011). Light enhances learned fear. Proc Natl Acad Sci U S A *108*, 13788-93.

51. Wouterlood, F.G., Saldana, E., Witter, M.P. (1990). Projection from the nucleus reuniens thalami to the hippocampal region: light and electron microscopic tracing study in the rat with the anterograde tracer Phaseolus vulgaris-leucoagglutinin. J Comp Neurol *296*,179-203.

52. Xu, W., and Südhof, T.C. (2013). A neural circuit for memory specificity and generalization. Science *339*, 1290-5.

53. Yamadera, H., Ito, T., Suzuki, H., Asayama, K., Ito, R., Endo, S. (2000). Effects of bright light on cognitive and sleep-wake (circadian) rhythm disturbances in Alzheimer-type dementia. Psychiatry Clin. Neurosci. *54*, 352–353.

54. Yamamoto, J., Suh, J., Takeuchi, D., Tonegawa, S. (2014). Successful execution of working memory linked to synchronized high-frequency gamma oscillations. Cell *157*, 845-57.

55. Zingg, B., Chou, X.L., Zhang, Z.G., Mesik, L., Liang, F., Tao, H.W., Zhang, LI. (2017). AAV-Mediated Anterograde Transsynaptic Tagging: Mapping Corticocollicular Input-Defined Neural Pathways for Defense Behaviours. Neuron *93*, 33-47.

FIGURES AND FIGURE LEGENDS

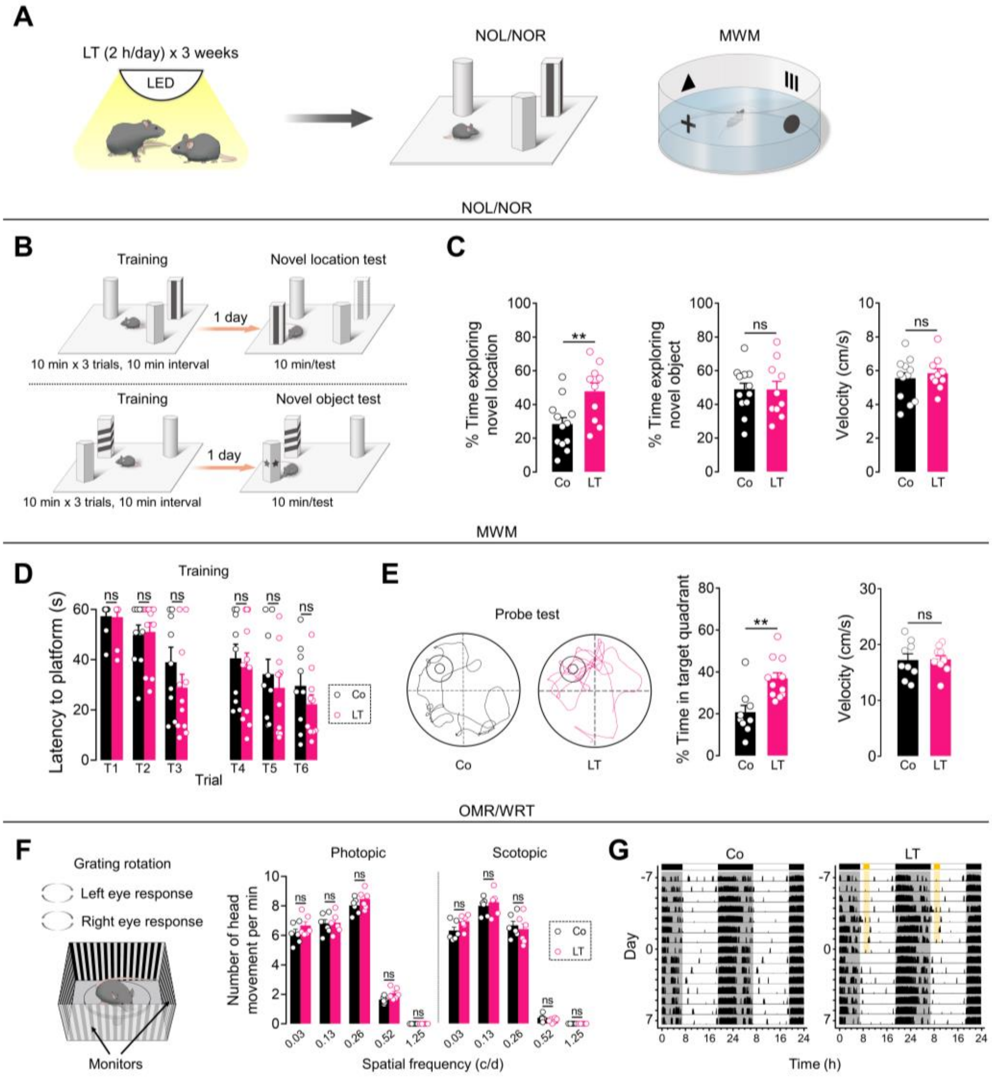

Figure 1. Long-term exposure to light treatment promotes spatial memory in the NOL and MWM tests

(**A**) Schematic of the experimental design. LT, light treatment. (**B**) Schematic of the novel object location (NOL) test and novel object recognition (NOR) test. (**C**) Left: recognition index of the NOL test. Middle: recognition index of the NOR test. Right: average velocity during the NOL test. Co (n=12 animals): mice that did not receive light treatment; LT (n=10 animals): mice that received 3 weeks of light treatment (3000 lux, 2 h/day). (**D**) Escape latencies (s) of Co (n=9 animals) and LT (n=11 animals) mice in the Morris water maze (MWM) test. (**E**) Left: swim paths in the probe test for representative animals in the Co and LT groups. The target quadrant is indicated by the annulus. Middle: percentage of time spent swimming in the target quadrant during the probe test of animals in the Co (n=9 animals) and LT (n=11 animals) groups. Right: average velocity during probe test of animals in the Co (n=9 animals) and LT (n=11 animals) groups. (**F**) Left: schematic of the experimental design. Right: the optomotor response of animals in the Co and LT groups (n=6 animals/group). (**G**) Representative double-plotted actograms showing wheel-running activities of mice in different experimental groups during a period of 7 days before and after the end of light treatment (day -7 to day 7). Co: mice that housed under a 7 AM to 7 PM 12 h:12 h light/dark cycle

(~200 lux white ambient illumination) for 3 weeks; LT: mice that housed under a 7 AM to 7 PM 12 h:12 h light/dark cycle (~200 lux white ambient illumination) except for during light treatment (3000 lux white ambient illumination between 8 AM to 10 AM) for 3 weeks. Yellow bars indicate turn on of bright light (3000 lux).

For all figures: One-way ANOVA with *Sidak`s* multiple comparisons test, **, *P*<0.001; ns=no significant difference. Error bars indicate the SEM.

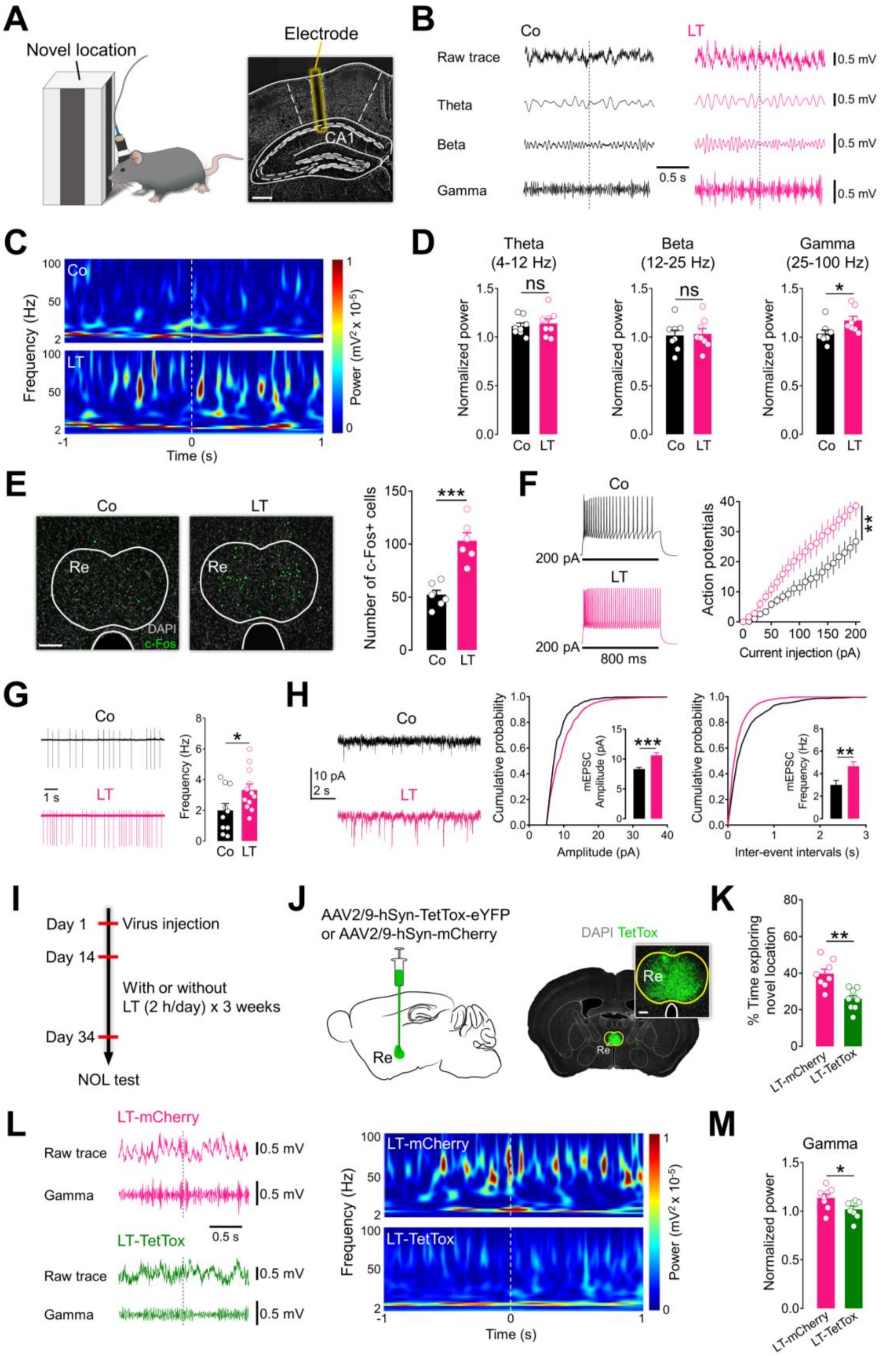

Figure 2. Activation of the Re is required for the spatial memory-promoting effects of light treatment

(**A**) Schematic of the experimental design. (**B**) Example local field potential (LFP) data as mice approached (<0 s) and explored (>0 s) a novel location. Co: mice that did not receive light treatment; LT: mice that received 3 weeks of light treatment (3000 lux, 2 h/day). (**C**) Moving window spectrograms for CA1 of the dorsal hippocampus (dHPC) time-locked to the initiation of novel location exploration (0 s). Minimum and maximum power values are noted on each spectrogram. (**D**) Mean theta, beta and gamma power while the mice explored the novel location (n=8 animals/group). (**E**) c-Fos expression in the Re in mice that did not receive light treatment (Co, n=6 animals), or received 3 weeks of light treatment (3000 lux, 2 h/day) (LT, n=6 animals). (**F**) The current-evoked action potentials in brain slices of mice in the Co and LT groups (n=12 cells/group). (**G**) Spontaneous firing in brain slices of mice in the Co (n=10 cells) and LT (n=12 cells) groups. (**H**) Cumulative distribution of mEPSC amplitude (left) or interevent interval and average frequency (right) of Re neurons in the Co (n=11 cells) and LT (n=13 cells) groups. (**I**) Schematic of the experimental design. LT: light treatment. (**J**) Scheme for infection of Re neurons with TetTox or mCherry. (**K**) Recognition index of the novel object location (NOL) test in different experimental groups (n=8 animals/group). All mice received 3 weeks of light treatment (3000 lux, 2 h/day). LT-mCherry: mice that received Re injection of AAV2/9-hSyn-mCherry; LT-TetTox: mice that received Re injection of AAV2/9-hSyn-TetTox-eYFP. (**L**) Left: example LFP data as mice in LT-mCherry and LT-TetTox groups approached (<0 s) and explored (>0 s) a novel location. Right: moving window spectrograms for CA1 of the dHPC time-locked to the initiation of novel location exploration (0 s). Minimum and maximum power values are noted on each spectrogram. (**M**) Mean gamma power while the mice explored the novel location (n=8 animals/group).

Sale bars: 200 µm (A); 100 µm (E and J). For all figures: One-way ANOVA with *Sidak`s* multiple comparisons test, *, *P*<0.05; **, *P*<0.001; ***, *P*<0.0001; ns=no significant difference. Error bars indicate the SEM.

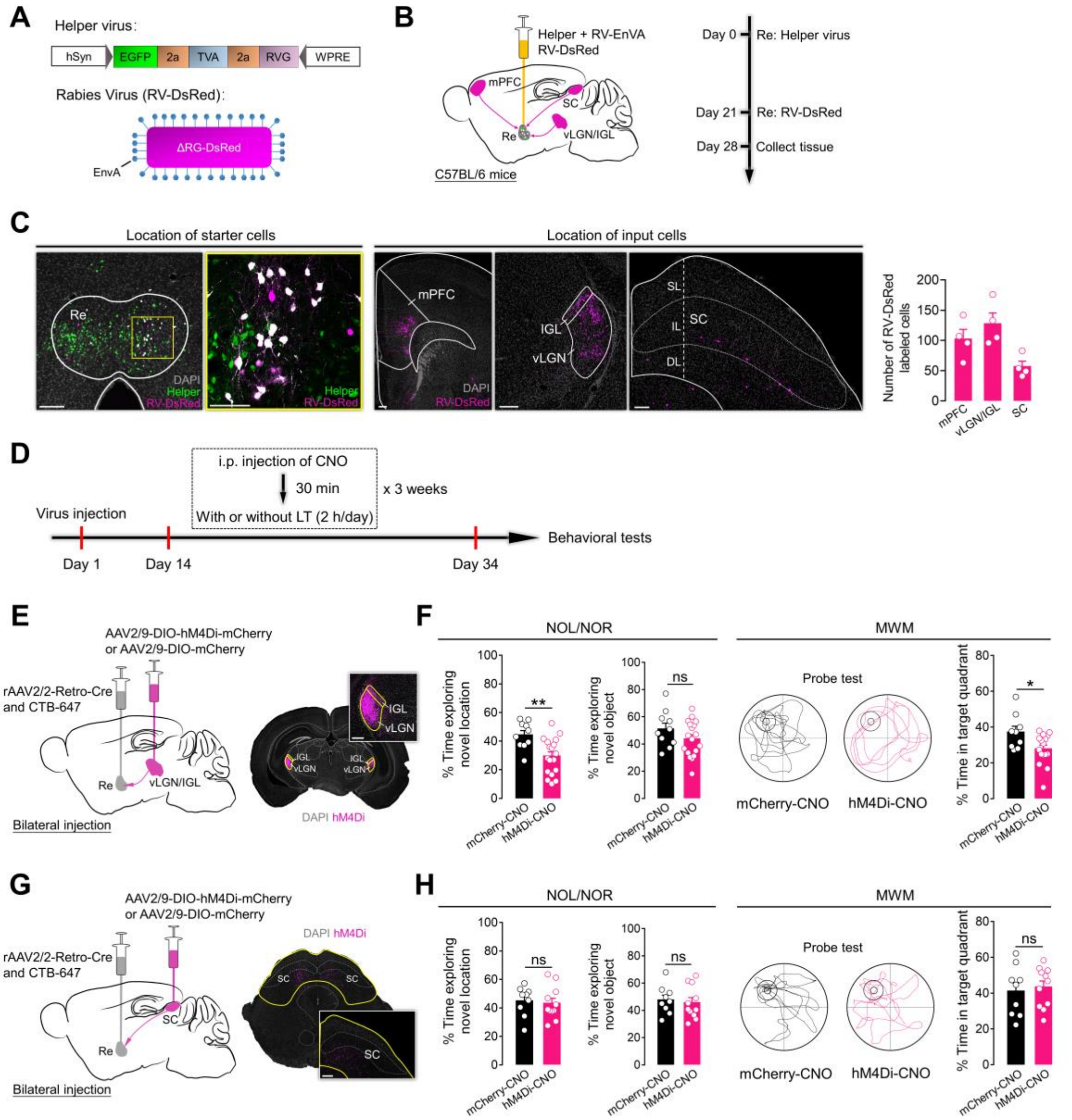

Figure 3. Activation of Re-projecting vLGN/IGL neurons is required for the spatial memory-promoting effects of light treatment

(**A**) Design of Helper virus and SAD-ΔG-DsRed (EnvA) (RV-DsRed). (**B**) Experimental design of virus tracing in C57BL/6 mice. (**C**) Left: injection site in the Re illustrating the location of starter cells (white). Right: representative images of the mPFC, vLGN/IGL, and SC showing the RV-DsRed-labeled cells. (**D**) Schematic of the experimental design. LT, light treatment. (**E**) Scheme for specific infection of Re-projecting vLGN/IGL neurons with hM4Di or mCherry. (**F**) Left: recognition indexes of the novel object location (NOL) and novel object recognition (NOR) tests in different experimental groups. All mice received Re injection of rAAV2/2-Retro-Cre and 3 weeks of light treatment (3000 lux, 2 h/day). mCherry-CNO (n=10 animals): mice that received vLGN/IGL injection of AAV2/9-DIO-mCherry and i.p. injection of CNO (1 mg/kg); hM4Di-CNO (n=18 animals): mice that received vLGN/IGL injection of AAV2/9-DIO-hM4Di-mCherry and i.p. injection of CNO (1 mg/kg). Right: swim paths and percent of time spent swimming in the target quadrant during the probe test of animals in the mCherry-CNO (n=9 animals) and hM4Di-CNO (n=16 animals) groups. (**G**) Scheme for specific infection of Re-projecting SC neurons with hM4Di or mCherry. (**H**) Left: recognition indexes of the NOL and NOR tests in different experimental groups. All mice received Re injection of rAAV2/2-Retro-Cre and 3 weeks of light treatment (3000 lux, 2 h/day). mCherry-CNO (n=9 animals): mice that received SC injection of AAV2/9-DIO-mCherry and i.p. injection of CNO (1 mg/kg); hM4Di-CNO (n=11 animals): mice that received SC injection of AAV2/9-DIO-hM4Di-mCherry and i.p. injection of CNO (1 mg/kg). Right: swim paths and percentage of time spent swimming in the target quadrant during the probe test of animals in the mCherry-CNO (n=9 animals) and hM4Di-CNO (n=11 animals) groups.

Scale bars: 200 µm (C, E, G). For all figures: One-way ANOVA with *Sidak`s* multiple comparisons test, *, $P<0.05$; **, $P<0.001$; ns=no significant difference. Error bars indicate the SEM.

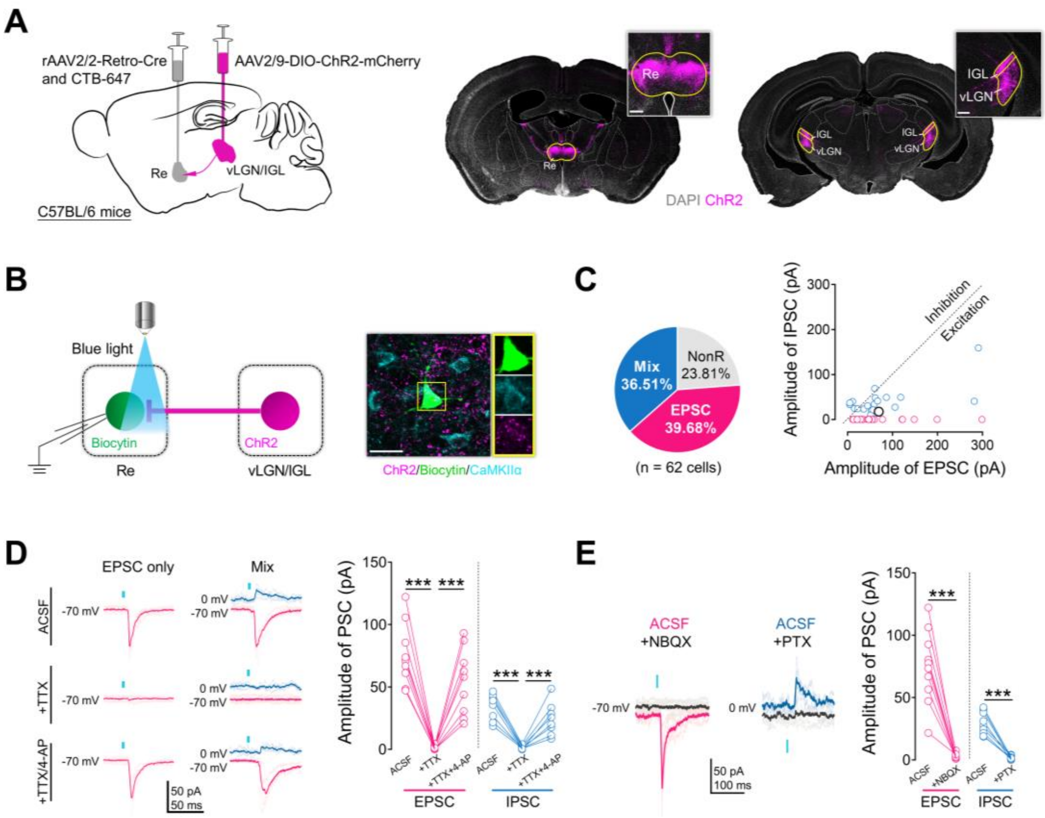

Figure 4. vLGN/IGL neurons activate the Re through direct projections

(**A**) Left: scheme for specific labeling of Re-projecting vLGN/IGL neurons with ChR2. Right: representative images of the vLGN/IGL and Re 2 weeks after virus injections. (**B**) Left: scheme for recording the postsynaptic currents in Re neurons evoked by optogenetic activation of vLGN/IGL-Re projections. Right: a recorded Re CaMKIIα neuron filled with biocytin. (**C**) Left: pie chart indicates whether the absolute amplitude was greater for evoked IPSCs, IPSCs and EPSCs (Mix) or no response. Right: absolute amplitude of optogenetically-evoked IPSCs and EPSCs in Re neurons (n=47 cells). (**D**) Optogenetically-evoked postsynaptic currents were completely blocked by the application of TTX and recovered by the application of TTX/4-AP. (**E**) Optogenetically-evoked EPSCs were blocked by the application of NBQX, while IPSCs were blocked by the application of PTX.

Sale bars: 200 µm (A-middle); 100 µm (A-right); 10 µm (B). For all figures: One-way ANOVA with *Sidak`s* multiple comparisons test, ***, $P<0.0001$. Error bars indicate the SEM.

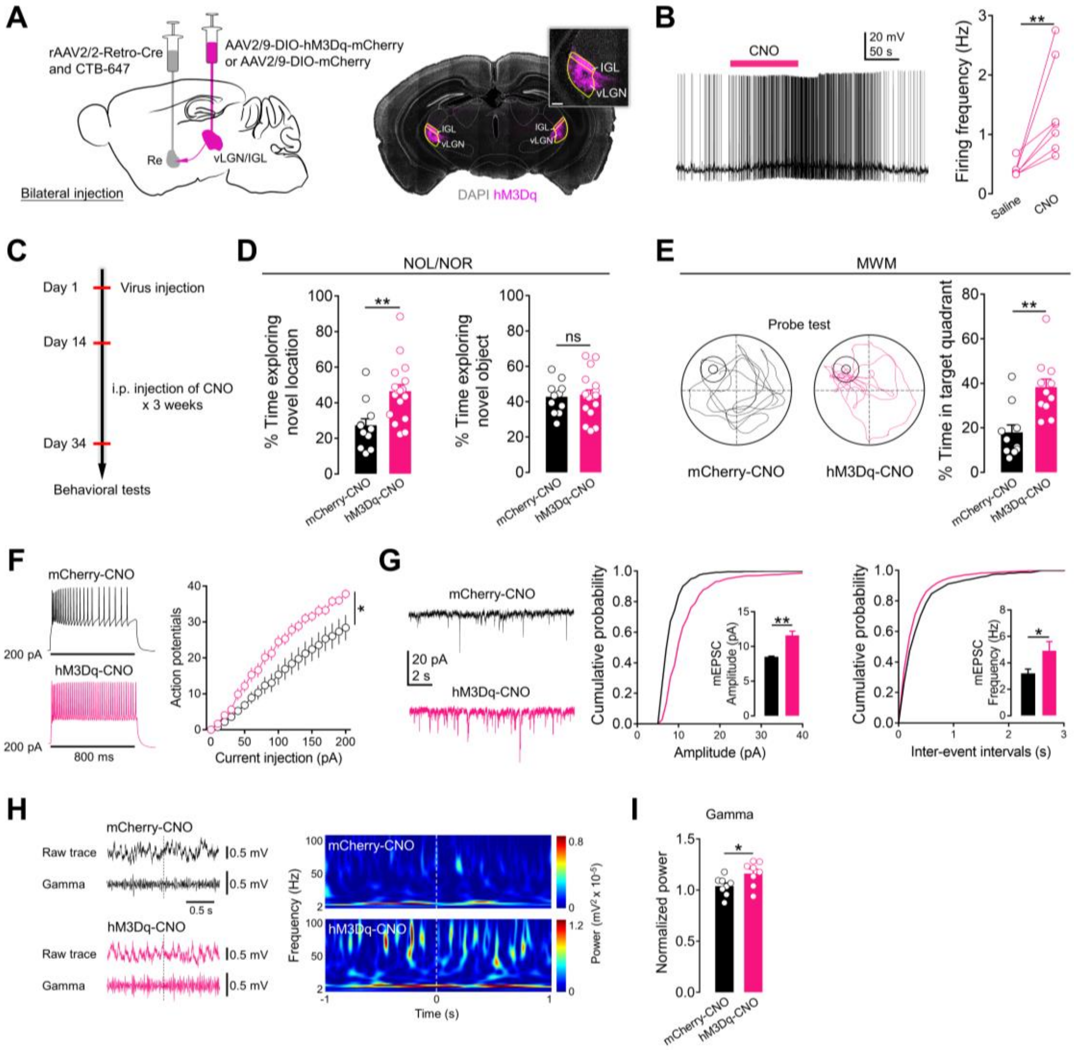

Figure 5. Activation of Re-projecting vLGN/IGL neurons promotes spatial memory

(**A**) Scheme for specific infection of Re-projecting vLGN/IGL neurons with hM3Dq or mCherry. (**B**) Re-projecting vLGN/IGL neurons expressing hM3Dq-mCherry can be activated by bath application of CNO (10 μM, 100 s). (**C**) Schematic of the experimental design. (**D**) Recognition indexes of the novel object location (NOL) and novel object recognition (NOR) tests in different experimental groups. All mice received Re injection of rAAV2/2-Retro-Cre. mCherry-CNO (n=11 animals): mice that received vLGN/IGL injection of AAV2/9-DIO-mCherry and i.p. injection of CNO (1 mg/kg); hM3Dq-CNO (n=17 animals): mice that received vLGN/IGL injection of AAV2/9-DIO-hM3Dq-mCherry and i.p. injection of CNO (1 mg/kg). (**E**) Swim paths and percentage of time spent swimming in the target quadrant during the probe test of mice in the mCherry-CNO (n=10 animals) and hM3Dq-CNO (n=11 animals) groups. (**F**) The current-evoked action potentials in brain slices of mice in the mCherry-CNO (n=12 cells) and hM3Dq-CNO (n=16 cells) groups. (**G**) Cumulative distribution of the mEPSC amplitude (left) or interevent interval and average frequency (right) of Re neurons in the mCherry-CNO (n=10 cells) and hM3Dq-CNO (n=14 cells) groups. (**H**) Left: example local field potential (LFP) data as mice in the mCherry-CNO and hM3Dq-CNO groups approached (<0 s) and explored (>0 s) a novel location. Right: moving window spectrograms for CA1 of the dHPC time-locked to the initiation of novel location exploration (0 s). Minimum and maximum power values are noted on each spectrogram. (**I**) Mean gamma power while the mice explored the novel location (n=8 animals/group).

Sale bar: 100 μm (A). For all figures: One-way ANOVA with *Sidak`s* multiple comparisons test, *, *P*<0.05; **, *P*<0.001; ns=no significant difference. Error bars indicate the SEM.

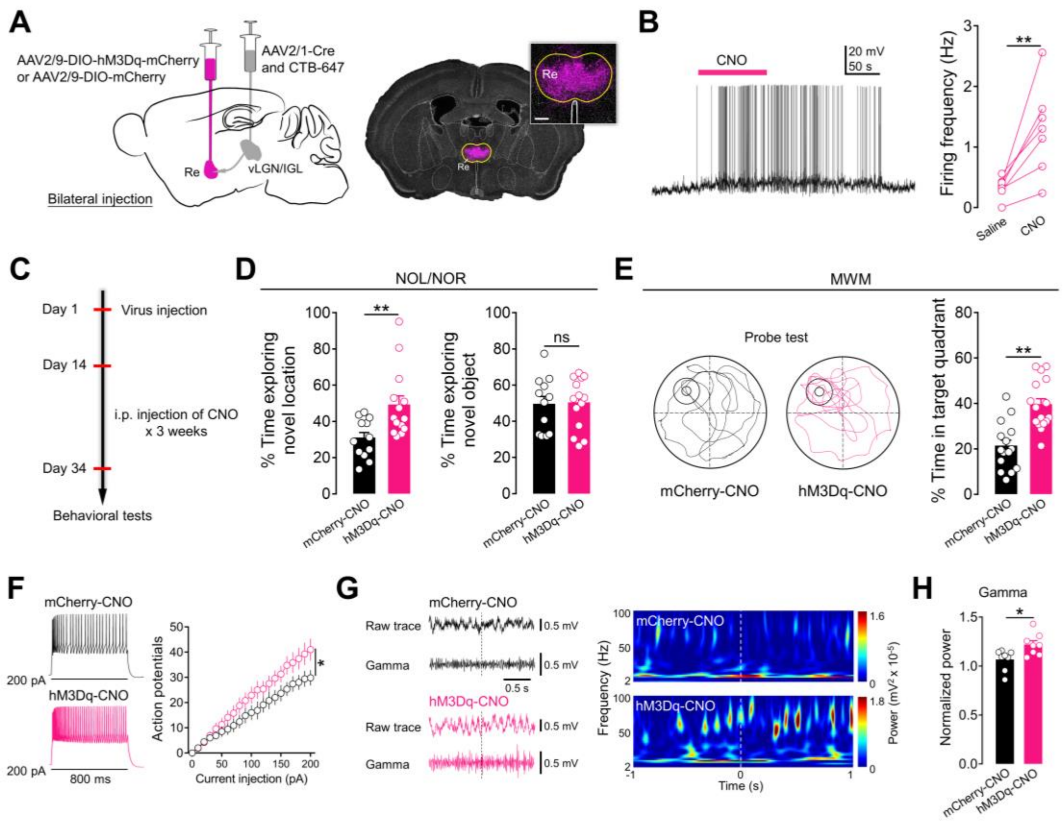

Figure 6. Activation of Re neurons receiving direct vLGN/IGL input promotes spatial memory (**A**) Scheme for specific infection of Re neurons receiving direct vLGN/IGL input (Re postsynaptic neurons) with hM3Dq or mCherry. (**B**) Re postsynaptic neurons expressing hM3Dq can be activated by bath application of CNO (10 μM, 100 s). (**C**) Schematic of the experimental design. (**D**) Recognition indexes of the novel object location (NOL) and novel object recognition (NOR) tests in different experimental groups. All mice received vLGN/IGL injection of AAV2/1-Cre. mCherry-CNO (n=12 animals): mice that received Re injection of AAV2/9-DIO-mCherry and i.p. injection of CNO (1 mg/kg); hM3Dq-CNO (n=14 animals): mice that received Re injection of AAV2/9-DIO-hM3Dq-mCherry and i.p. injection of CNO (1 mg/kg). (**E**) Swim paths and percentage of time spent swimming in the target quadrant during the probe test of mice in the mCherry-CNO (n=15 animals) and hM3Dq-CNO (n=16 animals) groups. (**F**) The current-evoked action potentials in brain slices of mice in the mCherry-CNO and hM3Dq-CNO groups (n=11 cells/group). (**G**) Left: example local field potential (LFP) data as mice in the mCherry-CNO and hM3Dq-CNO groups approached (<0 s) and explored (>0 s) a novel location. Right: moving window spectrograms for CA1 of the dHPC time-locked to the initiation of novel location exploration (0 s). Minimum and maximum power values are noted on each spectrogram. (**H**) Mean gamma power while the mice explored the novel location (n=8 animals/group).

Sale bar: 200 μm (A). For all figures: One-way ANOVA with *Sidak`s* multiple comparisons test, *, *P*<0.05; **, *P*<0.001; ns=no significant difference. Error bars indicate the SEM.

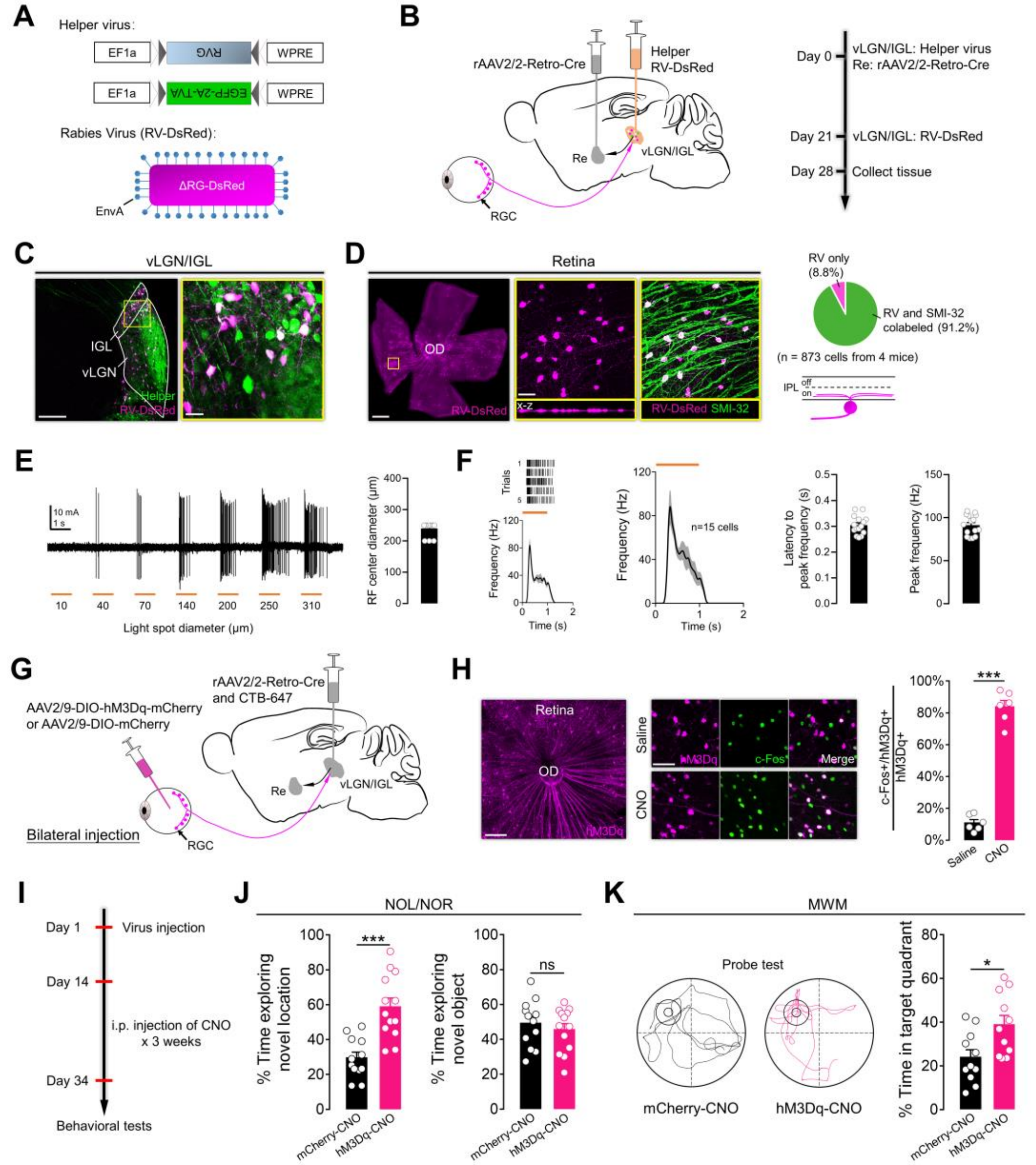

Figure 7. Activation of vLGN/IGL-projecting RGCs promotes spatial memory

(**A**) Design of Helper virus and SAD-ΔG-DsRed (EnvA) (RV-DsRed). (**B**) Experimental design of virus tracing in C57BL/6 mice. (**C**) Injection site of the vLGN/IGL illustrating the location of starter cells (white). (**D**) Left: a representative image of a whole-mount retina showing RV-DsRed-labeled RGCs that were immunopositive for SMI-32. Right-upper: pie chart indicates the percentage of RV-DsRed-labeled RGCs colabeled with SMI-32. Right-lower: schematic summary of the ramification pattern of RV-DsRed-labeled RGCs. IPL: inner plexiform layer; on: ON sublamina of the inner plexiform layer; off: OFF sublamina of the inner plexiform layer. (**E**) Left: responses of a RV-DsRed-labeled RGC to flashing spots (3.2 x 10^{10} photons/cm^2/s, 1 s on/1 s off) of increasing radius. Yellow bars indicate stimulus duration (1 s). Right: diameters of the RF centers of 15 recorded RGCs. (**F**) Left: raster plots and peri-stimulus time histogram (PSTH, bin size=50 ms) of a RV-DsRed-labeled RGC in response to a 1 s light spot (3.2 x 10^{10} photons/cm^2/s, 5 trials). Middle: mean PSTH (bin size=50 ms) of 15 RV-DsRed-labeled RGCs in response to a 1 s light spot (3.2 x 10^{10} photons/cm^2/s, 5 trials/cell). Yellow bars indicate stimulus duration (1 s). Right: latency from the light onset to the peak firing rate and the peak firing rate of 15 RV-DsRed-labeled RGCs in response to a 1 s light spot (3.2 x 10^{10} photons/cm^2/s). (**G**) Scheme for specific labeling of vLGN/IGL-projecting RGCs with hM3Dq-mCherry or mCherry. (**H**) Left: representative images of the retina showing i.p. injection of saline/CNO (1 mg/kg) evoked c-Fos expression in vLGN/IGL-projecting RGCs expressing hM3Dq. Right: the percentage of total hM3Dq RGCs expressing c-Fos in different groups (n=6 animals/group). (**I**) Schematic of the experimental design. (**J**) Recognition indexes of the novel object location (NOL) and novel object recognition (NOR) tests in different experimental groups. All mice received vLGN/IGL injection of rAAV2/2-Retro-Cre. mCherry-CNO (n=12 animals): mice that received intraocular injection of AAV2/9-DIO-mCherry and i.p. injection of CNO (1 mg/kg); hM3Dq-CNO (n=13 animals): mice that received intraocular injection of AAV2/9-DIO-hM3Dq-mCherry and i.p. injection of CNO (1 mg/kg). (**K**) Swim paths and percentage of time spent swimming in the target quadrant during the probe test of animals in the mCherry-CNO and hM3Dq-CNO groups (n=11 animals/group).

Scale bars: 200 μm (C-left); 20 μm (C-right); 1 mm (D-left); 50 μm (D-middle; H-right); 100 μm (H-left). For all figures: One-way ANOVA with *Sidak`s* multiple comparisons test, *, P<0.05; ***, P<0.0001; ns=no significant difference. Error bars indicate the SEM.

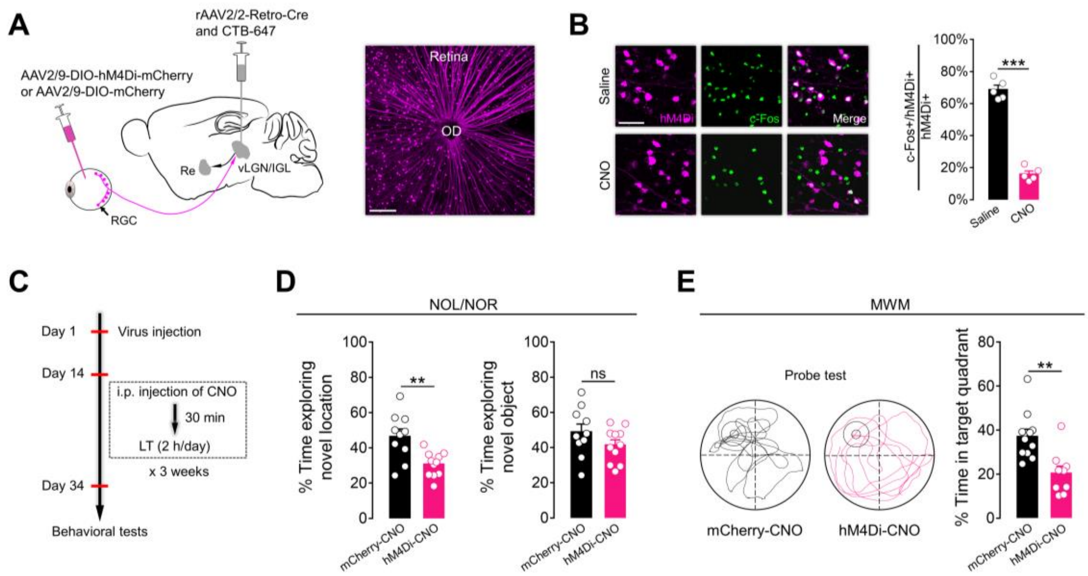

Figure 8. Activation of vLGN/IGL-projecting RGCs is required for the spatial memory-promoting effects of light treatment

(**A**) Scheme for specific labeling of vLGN/IGL-projecting RGCs with hM4Di-mCherry or mCherry. (**B**) Left: representative images of the retina showing that i.p. injection of CNO (1 mg/kg) decreased bright light (3000 lux, 2 h) induced c-Fos expression in vLGN/IGL-projecting RGCs expressing hM4Di. Right: the percentage of total hM4Di^{+} RGCs expressing c-Fos in different groups (n=5 animals/group). (**C**) Schematic of the experimental design. LT, light treatment. (**D**) Recognition indexes of the novel object location (NOL) and novel object recognition (NOR) tests in different experimental groups. All mice received vLGN/IGL injection of rAAV2/2-Retro-Cre and 3 weeks of light treatment (3000 lux, 2 h/day). mCherry-CNO (n=10 animals): mice that received intraocular injection of AAV2/9-DIO-mCherry and i.p. injection of CNO (1 mg/kg); hM4Di-CNO (n=11 animals): mice that received intraocular injection of AAV2/9-DIO-hM4Di-mCherry and i.p. injection of CNO (1 mg/kg). (**E**) Swim paths and percentage of time spent swimming in the target quadrant during the probe test of mice in the mCherry-CNO (n=11 animals) and hM4Di-CNO (n=9 animals) groups.

Scale bars: 100 μm (A); 50 μm (B); For all figures: One-way ANOVA with *Sidak`s* multiple comparisons test, **, P<0.001; ***, P<0.0001; ns=no significant difference. Error bars indicate the SEM.

STAR METHODS

RESOURCE AVAILABILITY

Lead Contact

Further information and request for resources and reagents should be directed to and will be fulfilled by the Lead Contact, Chaoran Ren (tchaoran@jnu.edu.cn).

Materials Availability

This study did not generate new plasmids or unique reagents.

This study did not generate new mouse lines.

Data and Code Availability

This study did not generate any unique datasets or code.

EXPERIMENTAL MODEL AND SUBJECT DETAILS

Mice

All experiments were approved by the Jinan University Institutional Animal Care and Use Committee. Adult (6-8 weeks old) male C57BL/6 mice, 6-month-old 5xFAD male mice were used in this study. The animals were housed in a 12 h:12 h light-dark cycle (lights on at 7 AM) with food and water provided *ad libitum*. The animals were randomly allocated to experimental and control groups. Experimenters were blind to the experimental group, and the order of testing was counterbalanced during behavioral experiments.

METHOD DETAILS

Surgery and intracranial injection

The mice were anesthetized (Avertin, 13 μl/g, i.p.) and placed in a stereotaxic instrument (RWD, Shenzhen, China). Erythromycin eye ointment was applied to prevent corneal drying and a heat pad (RWD, Shenzhen, China) was used to hold body temperature at 37 °C. A small craniotomy hole was made using a dental drill (OmniDrill35, WPI, Sarasota, FL), and injections were performed via a micropipette connected to a Nanoliter Injector (NANOLITER 2010, WPI, Sarasota, FL) and its controller (Micro4, WPI, Sarasota, FL) at a slow flow rate of 0.1 μl/min to avoid potential damage to local brain tissue.

To specifically infect vLGN/IGL CaMKIIα neurons with mCherry, AAV2/9-CaMKIIα-mCherry was injected into the vLGN/IGL of C57BL/6 mice (virus titres: 3.5 x 10^{12} GC/ml, 0.2 μl/injection; *AP*: -2.2 mm; *ML*: ± 2.5 mm; *DV*: -3.2 mm). Twenty-one days later, the green retrobeads (Lumafluor, US, 0.05 μl/injection) was injected into the Re (*AP*: -0.7 mm; *ML*: 0 mm; *DV*: -4.5 mm) of C57BL/6 mice.

To specifically infect Re-projecting vLGN/IGL neurons with ChR2-mCherry or mCherry or hM3Dq-mCherry or hM4Di-mCherry, rAAV2/2-Retro-Cre was injected into the Re of C57BL/6 mice (virus titres: 3 x 10^{12} GC/ml; 0.1 μl/injection), AAV2/9-DIO-ChR2-mCherry or AAV2/9-DIO-mCherry or AAV2/9-DIO-hM3Dq-mCherry or AAV2/9-DIO-hM4Di-mCherry was injected into the vLGN/IGL (virus titres: 3.5 x 10^{12} GC/ml, 0.2 μl/injection).

To specifically infect Re-projecting SC neurons with hM4Di-mCherry, rAAV2/2-Retro-Cre was injected into the Re of C57BL/6 mice (virus titres: 3 x 10^{12} GC/ml; 0.1 μl/injection), AAV2/9-DIO-hM4Di-mCherry was injected into the SC (virus titres: 3.5 x 10^{12} GC/ml, 0.2 μl/injection; *AP*: -3.7

mm; *ML*: ± 0.50 mm; *DV*: -1.3 mm).

To infect Re neurons with mCherry or TetTox-eYFP, AAV2/9-hSyn-mCherry or AAV2/9-hSyn-TetTox-eYFP (virus titres: 3.5 x 10^{12} GC/ml; 0.15 μl/injection) was injected into the Re of C57BL/6 mice.

To specifically infect postsynaptic Re neurons with mCherry or hM3Dq-mCherry, AAV2/1-Cre (virus titres: 1.5 x 10^{13} GC/ml; 0.1 μl/injection) was injected into the vLGN/IGL, AAV2/9-DIO-mCherry or AAV2/9-DIO-hM3Dq-mCherry was injected into the Re (0.15 μl/injection).

For monosynaptic tracing the inputs to Re, 0.15 μl Helper virus (rAAV2/9-hSyn-EGFP-2a-TVA-2a-RVG-WPRE-pA) (virus titres: 2 x 10^{8} GC/ml) was injected into the Re. Twenty-one days later, 0.1 μl of SAD-ΔG-DsRed (EnvA) (RV-DsRed, virus titres: 2 x 10^{8} GC/ml) was injected into Re.

For di-synaptic tracing retina→vLGN/IGL→Re pathway, 0.1 μl rAAV2/2-Retro-Cre was injected into the Re, and a total volume of 0.2 μl containing an equal volume of AAV2/9-EF1a-DIO-EGFP-TVA (virus titres: 2 x 10^{12} GC/ml) and AAV2/9-EF1a-DIO-RVG (virus titres: 2 x 10^{12} GC/ml) was injected at the vLGN/IGL. Twenty-one days later, 0.1 μl of SAD-ΔG-DsRed (EnvA) (RV-DsRed, virus titres: 2 x 10^{8} GC/ml) was injected into the vLGN/IGL.

To specifically infect the vLGN/IGL-projecting RGCs with mCherry or hM3Dq-mCherry or hM4Di-mCherry, 0.1 μl rAAV2/2-Retro-Cre was injected into the vLGN/IGL of C57BL/6 mice. AAV2/9-DIO-mCherry or AAV2/9-DIO-hM3Dq-mCherry or AAV2/9-DIO-hM4Di-mCherry was intraocularly injected (1.5 μl/eye).

Following injection, the micropipette was left in place for ~5 min and then extracted slowly (~1 min to completely move the micropipette from the injection site to the surface of the brain) to minimize virus leakage in the track. Finally, the wound was sutured, antibiotics (bacitracin and neomycin) were applied to the surgical wound and ketoprofen (5 mg/kg) was injected subcutaneously; the animals were allowed to recover from anesthesia under a heat lamp.

Injection site verification.

After transcardial perfusion with 0.9% saline followed by 4% paraformaldehyde in 0.1 M PBS, the brain was removed and post-fixed with 4% paraformaldehyde overnight at 4°C, and then transferred into 30% sucrose until sectioning with a cryostat (CM1900, Leica Microsystems, Bannockburn, IL). A series of 40 μm sections were collected for verification of injection sites. To confirm the injection sites of viruses that encoded a fluorescent protein (e.g., AAV2/9-DIO-hM3Dq-mCherry and AAV2/9-hSyn-TetTox-eYFP), coronal brain sections were examined under a fluorescence microscope (Zeiss, Axioimager Z2 microscope). Only mice with verified fluorescent protein expression were used for analysis. Mice with virus injections that missed the target area, fluorescent protein expression that was too low in the targeted area or extensively extended beyond the targeted area were excluded from the study. To visualize the injection sites of viruses that did not encode fluorescent protein (i.e., rAAV2/2-Retro-Cre and AAV2/1-Cre), Alexa Fluor 647-conjugated cholera toxin subunit B (CTB-647, 0.05 μl/injection) was injected into the targeted regions along with the viruses. The location of the virus injection site was visualized with CTB-647. Only mice with verified injection sites were used for analysis.

Physiological recording from brain slices.

For brain slice preparation, the mice were deeply anesthetized with isoflurane, and coronal sections (250 μm thick) containing the Re were cut using a vibratome (VT1200S; Leica Microsystems) in ice-cold artificial cerebrospinal fluid (ACSF, in mM: 119 NaCl; 2.5 KCl, 1 NaH_2PO_4, 11 glucose, 26.2 $NaHCo_3$, 2.5 $CaCl_2$, 1.3 $MgCl_2$, and 290 mOsm, at pH 7.4). The brain slices were recovered for ~1 h at room temperature in ACSF. After recovery, the slices were placed in the recording chamber and continuously perfused with ACSF.

Evoked postsynaptic currents were elicited by 2 ms blue light stimulation of axonal terminals of Re-projecting vLGN/IGL neurons infected with ChR2-mCherry. Blue-light-evoked EPSCs and IPSCs were recorded when the membrane potential was held at -70 mV and 0 mV, respectively. To test whether the recorded IPSCs were mediated by the GABA receptor, 100 μM picrotoxin was added to ACSF. To test whether the recorded EPSCs were mediated by the AMPA/kainate receptor, 10 μM NBQX was added to ACSF. To test whether the postsynaptic currents recorded in Re neurons were elicited by direct synaptic connections, 1 μM tetrodotoxin (TTX) and 100 μM 4-aminopyridine (4-AP) were added to ACSF. The recorded cells were intracellularly filled with biocytin for morphological evaluation.

To measure the excitability of Re neurons, electrodes were filled with K^+-based peptide solution (in mM: 130 $KMeSO_4$, 10 KCl, 10 Na_2-phosphocreatine, 4 MgATP, 0.3 Na_3GTP, 10 HEPES, 290 mOsm, adjusted to 7.4 with KOH). A depolarizing current was applied (0.8 s for 200 pA) from a membrane potential of -70 mV.

To record the mini excitatory postsynaptic currents (mEPSCs) of Re neurons, 1 μM TTX was added to ACSF, electrodes were filled with Cs^+-based peptide solution (in mM: 130 $CsMeSO_4$, 10 NaCl, 10 EGTA, 4 MgATP, 0.3 Na_3GTP, 10 HEPES, 290 mOsm, adjusted to 7.4 with CsOH), and the membrane potential was held at -70 mV. Spontaneous firings were recorded with ACSF in the electrodes.

To measure the function of chemogenetic viruses, neurons expressing hM3Dq-mCherry or hM4Di-mCherry in the SC, vLGN/IGL or Re were recorded. For chemogenetic activation, neurons were recorded in the current-clamp model. After 80 s of baseline recording, 10 μM CNO was washed into ACSF for 100 s, and the neurons were recorded for 4 min in total. For chemogenetic inhibition, mCherry-labeled neurons were injected with a 100 pA current, and the number of activated action potentials was calculated as the baseline. Then, 10 μM CNO was added to ACSF for 10 min, and the action potentials activated by 100 pA current injection were recorded. Finally, the CNO was washed out, and the activated action potentials were recorded.

For whole-mounted retinal preparation, the animal was dark adapted for 40 min before enucleation and under dim red light, the lens and vitreous were carefully removed with a pair of fine-forceps. The eyecup was flat mounted, sclera side down, directly on the bottom of a recording chamber and was superfused by oxygenated (95% O_2/5% CO_2) Ames medium (Sigma-Aldrich, St. Louis, MO) at a fixed rate (5 ml/min) at room temperature. Visual responses of the rabies virus-labeled RGCs were recorded extracellularly using a glass microelectrode. The receptive field (RF) was mapped with a 0.2° test spot. To assess the RF centers of the recorded RGCs, a circular light spot (3.2 x 10^{10} photons/cm^2/s) centered on the cell body was flashed on and off periodically (1 s on/1 s off). The spot size gradually increased (spot diameters: 10, 40, 70, 140, 200, 250 and 310 μm). The spot size that could evoke the maximum discharge was accepted as covering the RF center. After 40 min of dark adaptation, the dynamics of the light response were assessed by inspecting the time course of the firing rate under a 1 s light spot (3.2 x 10^{10} photons/cm^2/s, 5 trials/cell) with a size equal to the RF center of the recorded RGC. Peri-stimulus time histogram (PSTH) was generated in Matlab with 50 ms bins.

All recordings were performed using a Multiclamp 700B amplifier (Molecular Devices). Traces were low-pass-filtered at 2 kHz and digitized at 10 kHz. For light stimulation, light pulses were delivered through digital commands from the Digidata 1550A and Digital stimulator (PG4000a, Cygnus Technology). The pipette resistance ranged from 4 to 6 MΩ. When stable whole-cell recordings were achieved with an access resistance below 25 MΩ, basic electrophysiological properties were recorded. Offline data analysis was performed using Clampfit 10.0 software (Molecular Devices).

***In vivo* LFPs**

LFP recordings were performed as described in previous studies with minor modifications. The mice were deeply anesthetized with isoflurane, and a 75-μm stainless-steel electrode (Cat No. 791000, A-M system, USA) was subsequently positioned in the principal cell layer of CA1 of the dorsal HPC (*AP*: -1.82 mm; *ML*: +1.25 mm; *DV*: -1.38 mm). After surgery, the mice were given at least 7 days to recover. Recording signals were digitized at 30 kHz by the NeuroLego System (Jiangsu Brain Medical Technology Co. Ltd.), and then resampled at 1 kHz for the LFP analysis. The videos were recorded simultaneously with a camera (Hikvision, China). LFP data analyses were computed with the Matlab spectrogram function at a resolution of $\Delta F = 2$ Hz and $\Delta T = 1$ ms. The time window of the NOL event was defined as the period 1 s before and after the nose-poke of the familiar object in the novel location. The normalized power change of the theta (4-12 Hz), beta (12-25 Hz), and gamma (25-100 Hz) rhythm was defined as the mean power at every point divided by the mean of the baseline (2 s before the time window of the NOL event).

Immunocytochemistry

All animals were anesthetized (Avertin, 13 μl/g, intraperitoneally) and perfused intracardially with 0.9% saline followed by 4% paraformaldehyde in phosphate-buffered saline (PBS). Brains and eyes were removed.

For CaMKIIα labeling, 40 μm cryostat sections containing the Re were placed in blocking solution for 1 h before incubation in primary antibody against CaMKIIα (rabbit, 1:500; ab5683, Abcam) (36 h at 4 °C). Sections were then incubated with corresponding secondary antibody at a dilution of 1:400 for 6 h at room temperature: (Dylight 647) goat-anti-rabbit IgG (DI-1649, Vector Laboratories).

For detection of biocytin-filled Re neurons, cryostat sections containing the Re were placed in 0.1 M PBS containing 10% normal goat serum (Vector Laboratories, Burlingame, CA) and 0.3% Triton X-100 (T8787, Sigma-Aldrich, St Louis, MO) for 1 h before incubation in Streptavidin-Alexa Fluor 488 (1:100, S32354, Thermo Fisher Scientific) for 48 h at 4 °C.

For c-Fos labeling, procedures used in CaMKIIα labeling were adopted except that the primary antibody was replaced by antibody against c-Fos (rabbit, 1:500; 2250, Cell signaling technology), and the secondary antibody was replaced by goat anti-rabbit Alexa 488 (1:400, 111-545-003, Jackson ImmunoResearch).

For detection of SMI-32 expressing RGCs, retinas were isolated and washed in 0.1 M PBS for 3 times (10 min each) before incubation in 0.1 M PBS containing 10% normal goat serum (Vector Laboratories, Burlingame, CA) and 0.3% Trition-X-100 (T8787, Sigma-Aldrich, St Louis, MO) for 1 hour. Then retinas were incubated for 3 days at 4 °C with a mouse anti-SMI-32 antibody (1:1000, 801703, Biolegend). This was followed by 6 rinses in 0.1 M PBS and then incubation with a secondary (Dylight 594) goat-anti-mouse IgG (1:400, 35510, Thermo Fisher Scientific) for 6 hours at room temperature.

Finally, all sections and retinas were rinsed in 0.1M PBS and cover-slipped in anti-fading aqueous mounting medium with DAPI (EMS, Hatfield, PA).

Image analysis.

Retinas and sections were imaged with a Zeiss 700 confocal microscope with 5x or 20x objectives, or a 40x oil immersion objective. For three-dimensional reconstruction of injected or virus labeled cells, optical sections were collected at 0.2 μm intervals. Each stack of optical sections covered a retinal area of 325.75 × 325.75 mm^2 (1024 ×1024 pixels). Using Image J and Photoshop CS5 (Adobe Corp., San Jose, California, USA), each stack of optical sections was montaged and projected to a 0° X-Y plane and a 90° Y-Z plane to obtain a three-dimensional reconstruction of the cell. Contrast and brightness were adjusted, and the red-green images had been converted to magenta-green. Total soma and dendritic field size of each rabies virus labeled RGCs were analyzed. Dendritic field area was calculated by drawing a convex polygon linking the dendritic terminals. The dendritic field area was then calculated, and the diameter expressed as that of a circle having an equal area.

Behavioral paradigms.

Behavioral tests were performed during the light phase (1 PM to 4 PM) unless otherwise specified. Operators were blinded to the experimental group during scoring.

Light treatment

The animals in both the control and light treatment groups were kept in their home cages which were placed on different layer of a custom-designed light cabinet for different time period (1 day, 1 week, 2 weeks, 3 weeks, or 4 weeks), where all animals were housed at room temperature with *ad libitum* access to food and water. Cool LED lights (UV-free) with adjustable brightness was installed at the top of each floor of the cabinet so that the brightness of each floor of the cabinet could be adjusted manually (the light intensity was determined by averaging the measurements from the top and the four sides of the cage). The animals in the control group were housed under a 7 AM to 7 PM 12 h:12 h light/dark cycle (~200 lux white ambient illumination). The animals in the experimental group were also housed under a 7 AM to 7 PM 12 h:12 h light/dark cycle (~200 lux white ambient illumination) except for during light treatment (~0 lux or 1000 lux or 3000 lux or 5000 lux white ambient illumination between 8 AM and 10 AM, or ~3000 lux white ambient illumination between 1 PM and 3 PM). Following housing in the light cabinet, all animals underwent behavioral tests as detailed below.

Novel object location/novel object recognition (NOL/NOR) test

The mice were habituated to the experimental room for 3 consecutive days before the training phase, during which the mice were allowed to freely explore the white Plexiglas arena (50 cm length × 50 cm width × 40 cm height) with dim light (~15 lux) for 10 min per day. For the training, three distinct objects were placed in 3 corners of the arena 10 cm from the wall. The mice were allowed to explore the objects for 10 min for 3 trials, and each trial was separated by 10 min. Memory of the location or object was tested 24 h after training. For the NOL test, one of the objects was moved to the diagonal position, and the percentage of time that the mice spent exploring the novel location in 10 min was calculated as the capacity for location memory. For the NOR test, one of the familiar objects was replaced by a novel object that was different from the familiar ones, and the locations of these objects were unchanged. The percentage of time that the mice spent exploring the novel object in 10 min was calculated as the capacity for memory of the object. All objects were previously screened, and the mice showed no significant preference for these objects. The arena and objects were wiped clean with a paper towel soaked in 50% ethanol and dried thoroughly after each test session.

Open field test (OFT)

Motor activity was measured in a white Plexiglas arena (50 cm length × 50 cm width × 40 cm height) during the first habituation phase of the NOL/NOR test. Briefly, the mice were placed in the center of a plastic box with dim light (~15 lux) and were allowed to explore the arena for 10 min. All animal activity was recorded with an infrared camera placed above the box. Locomotion and time spent in the center during the 10 min of exploration was measured (Ethovision XT software). The box was wiped clean with a paper towel soaked in 50% ethanol and dried thoroughly after each test session.

To test the response of mice to bright light when challenged with the OFT and NOL test (Figures S9J and S9K), 16 mice were divided into 2 groups: Co (n=8 animals): the mice were first challenged with the OFT in dim light (~15 lux). Three days later, the mice were challenged with the NOL test in dim light (~15 lux); BL (n=8 animals): the mice were first challenged with the OFT in bright light (1000 lux). Three days later, the mice were challenged with the NOL test, in which bright light (1000 lux) was turned on during the training and testing phases. In this experiment, the OFT and NOL test were performed between 8 PM and 11 PM.

MWM test

Spatial learning was assessed with the hidden platform version of the MWM test. The test apparatus consisted of a large circular pool (diameter 120 cm, depth 70 cm) filled with water (25–26 °C) to a depth of 40 cm. The water was made opaque with milk to prevent the animals from seeing the circular platform (diameter 12 cm) submerged 1 cm beneath the water surface. The platform was located at a fixed spatial position in one of the quadrants 20 cm from the pool wall. The pool was divided into 4 quadrants with distinct visual cues fixed onto the pool wall.

Twenty-four hours prior to the start of training, all mice were habituated to the pool by allowing them to perform a 60 s swim without the platform. In the following 2 days, the mice were trained to find the hidden platform in a fixed quadrant. Mice received 1 training session per day, which contained 3 trials. The trials in each session were separated by a 15 min break. For each trial, the mice were gently released into the pool, facing the wall. The mice were given a maximum of 60 s to find the platform. After finding the platform, they were allowed to remain there for 12 s and were then placed in a holding cage until the start of the next trial. The animals that failed to find the platform in 60 s were placed on the platform and allowed to rest for 12 s. Latency to platform and swimming speed were collected for subsequent analysis. After completion of training, the animals were returned to their home cages until the probe test 24 h later. The probe test consisted of a 60 s free swim period without a platform in which the time spent in the target quadrant was recorded.

Optomotor test

The mice were placed on a platform in the form of a grid (12 cm diameter, 19 cm above the bottom of the drum) surrounded by a motorized drum (29 cm diameter) that could be revolved clock-wise or anticlockwise at two revolutions per min. After 10 min of adaptation in the dark, vertical black and white stripes of a defined spatial frequency were presented to the animal. These stripes were rotated alternately clockwise and anticlockwise, for 2 min in each direction with an interval of 30 s between the two rotations. Various spatial frequencies subtending 0.03, 0.13, 0.26, 0.52 and 1.25

cycles/degree were tested individually on different days in a random sequence. The animals were videotaped with an infrared digital video camera for subsequent scoring of head tracking movements. Procedures for measuring optomotor responses under photopic condition was similar to the scotopic condition except that animals were subjected to 400 lux during 5 min to allow them to adapt to the light.

Wheel-running test (WRT)

Twenty-four mice were randomly divided into two groups (n=12 animals/group) and were individually housed in cages equipped with a running wheel (110 mm diameter). Cool LED lights (UV-free) with adjustable brightness were installed at the top of each cage. All animals were housed at room temperature with *ad libitum* access to food and water. The animals in the control group (Co, n=12 animals) were housed under a 7 AM to 7 PM 12 h:12 h light/dark cycle (~200 lux white ambient illumination). The animals in the experimental group (LT, n=12 animals) were also housed under a 7 AM to 7 PM 12 h:12 h light/dark cycle (~200 lux white ambient illumination) except for during light treatment (3000 lux white ambient illumination between 8 AM and 10 AM, from day -20 to day 0) (day 0 = the last day of 3 weeks light treatment). The number of wheel revolutions was counted by a custom-made drive based on ArControl (Chen and Li, 2017). The activity onset and locomotor activity in 5 min time bins during a period of 7 days before and after the end of light treatment (day -7 to day 7) were analyzed using Matlab and GraphPad software.

Sucrose preference test (SPT)

The mice were tested for preference for a 2% sucrose solution (Sucrose, Sigma-Aldrich) using a two-bottle choice procedure. Each animal was housed individually during the 2-day test period. The animals were given two bottles, one of sucrose and one of tap water. Every 24 h, the amounts of sucrose and water consumed were recorded. To prevent potential location preference for drinking, the positions of the bottles were changed every 24 h. Food and water were available *ad libitum* prior to the SPT. The preference for the sucrose solution was determined as the percentage of sucrose solution ingested relative to the total intake.

QUANTIFICATION AND STATISTICAL ANALYSIS

Quantification of neurons infected with different viruses.

To quantify percentage of Re-projecting vLGN/IGL neurons colabeled with mCherry and retrobeads (Figure S4E), 3 C57BL/6 mice received vLGN/IGL injection of AAV2/9-CaMKIIα-mCherry and Re injection of green retrobeads were used. In each mouse, the number of mCherry-labeled neurons and mCherry/retrobeads double labeled neurons were counted in 4 serial brain sections (40 μm/section) across the vLGN/IGL. The percentage of mCherry/retrobeads double labeled neurons was calculated as a percentage of the total number of mCherry/retrobeads double labeled neurons counted in 3 mice from the total number of retrobeads-labeled neurons counted in 3 mice.

To quantify the number of the RV-DsRed labeled presynaptic neurons in the mPFC and vLGN/IGL and SC (Figure 3C), 4 C57BL/6 mice received Re injection of helper virus and RV-DsRed were used. In each mouse, the number of RV-DsRed labeled mPFC, vLGN/IGL and SC neurons from 4 serial brain sections (40 μm/section) across the mPFC, vLGN/IGL, and SC were counted.

To quantify percentage of RV-DsRed labeled RGCs co-labeled with SMI-32 (Figure 7D), 4 C57BL/6 mice received vLGN/IGL injection of helper virus and RV-DsRed were used. In each mouse, the number of RV-DsRed-labeled RGCs and RV-DsRed/SMI-32 double labeled RGCs were counted in the contralateral retina. The percentage of RV-DsRed/SMI-32 double labeled RGCs was calculated as a percentage of the total number of RV-DsRed/SMI-32 double labeled RGCs counted in 4 mice from the total number of RV-DsRed-labeled RGCs counted in 4 mice.

Quantification of c-Fos immunostaining.

To quantify the influence of 3 weeks of light treatment on c-Fos expression in the Re, dorsal HPC (dHPC), vLGN/IGL and SC (Figure 2E; Figure S2A), 12 C57BL/6 mice were divided into 2 groups: 1) Co, 6 mice were housed under a 7 AM to 7 PM 12 h:12 h light/dark cycle (~200 lux white ambient illumination); 2) LT, 6 mice were housed under a 7 AM to 7 PM 12 h:12 h light/dark cycle (~200 lux white ambient illumination) except for during light treatment (~3000 lux white ambient illumination between 8 AM and 10 AM). Three weeks later, the animals in the LT group were anesthetized and perfused after the last session of light treatment (between 10 AM and 10:30 AM), and the animals in the Co group were also anesthetized and perfused during the same time period. Brain slices across the dHPC, Re, vLGN/IGL, and SC were subjected to immunostaining of c-Fos. In each mouse, the number of c-Fos labeled neurons were counted from 4 serial brain sections (40 μm/section) across the dHPC, Re, vLGN/IGL, and SC. The average number of c-Fos$^+$ cells in the dHPC, Re, vLGN/IGL, and SC was calculated as the total number of c-Fos$^+$ cells counted in 6 animals divided by the number of animals.

To quantify the influence of chemogenetic activation of the vLGN/IGL-projecting RGCs on c-Fos expression (Figure 7H), 12 C57BL/6 mice received vLGN/IGL injection of rAAV2/2-Retro-Cre and intraocular injection of AAV2/9-DIO-hM3Dq-mCherry were divided into 2 groups: 1) Saline, 6 mice received i.p. injection of saline, followed by a 30 min interval and then received light deprivation (2 h); 2) CNO, 6 mice received i.p. injection of CNO (1 mg/kg), followed by a 30 min interval and then received light deprivation (2 h). All animals were anesthetized and perfused. Retinas were subjected to immunostaining of c-Fos. In each mouse, the number of hM3Dq-labeled RGCs and c-Fos/hM3Dq double labeled RGCs were counted from 4 randomly selected equivalent areas of retina. The percentage of c-Fos/hM3Dq double-labeled RGCs in each group was calculated as the percentage of the total number of c-Fos/hM3Dq double-labeled RGCs counted in 6 mice within the total number of hM3Dq-labeled RGCs counted in 6 mice.

To quantify the influence of chemogenetic inhibition of the vLGN/IGL-projecting RGCs on c-Fos expression (Figure 8B), 10 C57BL/6 mice received vLGN/IGL injection of rAAV2/2-Retro-Cre and intraocular injection of AAV2/9-DIO-hM4Di-mCherry were divided into 2 groups: 1) Saline, 5 mice received i.p. injection of saline and exposure to bright light (3000 lux, 2 h); 2) CNO, 5 mice received i.p. injection of CNO (1 mg/kg) and exposure to bright light (3000 lux, 2 h). All animals were anaesthetized and perfused. Retinas were subjected to immunostaining of c-Fos. In each mouse, the number of hM4Di-labeled RGCs and c-Fos/hM4Di double labeled RGCs were counted from 4 randomly selected equivalent areas of retina. The percentage of c-Fos/hM4Di double-labeled RGCs in each group was calculated as the percentage of the total number of c-Fos/hM4Di double-labeled RGCs counted in 5 mice within the total number of hM4Di-labeled RGCs counted in 5 mice.

Statistics.

All statistics were calculated using GraphPad Prism 7 software. Data analysis was done by experimenters blind to experimental conditions. Statistical details including the definitions and exact value of n (e.g., number of animals, etc.), p values, and the types of the statistical tests can be found in the Figures and Figure legends. One-way ANOVA and then *Sidak`s* multiple comparisons test was used to quantify the performance of the NOL, NOR, MWM, OFT, SPT, OMR, and WRT tests, the amplitude and frequency of mEPSC, number of action potentials activated by current injection, and spontaneous firing frequency of Re neurons. For all figures, dot plots include horizontal line representing mean. Statistical significance was set at $P<0.05$.